Cuaternario y Geomorfología
ISSN: 0214-1744
ISSNe: 2695-8589

www.rediris.es/CuaternarioyGeomorfologia/

Spatial patterns of exposure to sediment-laden flows on an experimental alluvial fan

Patrones espaciales de exposición a flujos cargados de sedimento en un abanico aluvial experimental

Blasi, Alessio [(1)], Mazzorana, Bruno [(2), (3)]*, Sturm, Michael [(4)], Gems, Bernhard [(5)]

(1) Free University of Bozen-Bolzano, Faculty of Science and Technology, Bolzano 39100, Italy.
(2) Universidad Austral de Chile, Faculty of Sciences, Instituto de Ciencias de la Tierra, Valdivia 5090000, Chile.
(3) Universidad Austral de Chile, RINA, Natural and Anthropogenic Risks Research Center, Valdivia 5090000, Chile.
(4) Department of Water Management, Office of the Tyrolean Regional Government, Imst 6460, Austria.
(5) University of Innsbruck, Unit of Hydraulic Engineering, Innsbruck 6020, Austria.

Abstract

Sediment-laden flows with significant amounts of large wood can impact alluvial fans and seriously damage infrastructure and property which makes a profound knowledge of exposure an essential requisite for risk mitigation. To investigate its spatial variability, we executed experiments on a simplified physical model and assessed the observed spatial process and exposure patterns by quantifying synthetic indexes and geostatistically analysing spatial probabilities. We systematically varied the loading conditions, i.e. total flow volume, solid fraction and the tank opening controlling water release, and repeated each experimental configuration eight times. Two alluvial fan layouts were considered, one equipped with a guiding channel and a bridge and one with a guiding channel only. First, we tested the hypothesis, that water released though the fully opened tank outflow valve induces a sediment-laden flow which is associated with higher exposure and lower spatial uncertainty of exposure if compared to flows generated by a half-opened tank outflow valve. Second, we tested whether a higher flow volume is associated with higher exposure on the alluvial fan and with lower spatial uncertainty. It turned out that neither of the aforementioned hypotheses is verified for the whole set of tested flow conditions. The first hypothesis is rejected in the majority of the considered conditions. The second hypothesis is prevailingly corroborated when the exposed areas due to both sediment and water were considered. Instead, when only the areas of sediment deposition are considered, this hypothesis is prevailingly corroborated on the alluvial fan featuring the presence of the bridge. We provided exposure probability

* Corresponding author: Bruno Mazzorana – tel: 0056966515334; email: bruno.mazzorana@uach.cl; address: Campus Isla 9 Teja, Edificio Pugin, office 339, 5090000, Valdivia, Chile.

https://doi.org/10.17735/cyg.v37i1-2.95210

maps for all experimental conditions and presented the variability of exposure by standard deviation ellipses. Although solely indicative for the adopted alluvial fan layouts, a variation of the loading parameters led to remarkable changes in the patterns of exposure probability and the parameters of the standard deviation ellipses. Our results urge decision makers to fully acknowledge the potential variability of geomorphic responses on alluvial fans in their risk management practices as to avoid underestimating the impacts for the built environment.

Keywords: alluvial fan, fluvial hazards, exposure, modelling.

Resumen

Los flujos cargados de sedimentos con cantidades significativas de madera de gran tamaño pueden afectar a los abanicos aluviales y dañar seriamente la infraestructura y la propiedad expuesta, lo que hace que un conocimiento profundo de la exposición sea un requisito esencial para la mitigación del riesgo. Para investigar su variabilidad espacial, ejecutamos experimentos en un modelo físico simplificado y evaluamos el proceso espacial observado y los patrones de exposición cuantificando índices sintéticos y analizando geoestadísticamente las probabilidades espaciales de ocurrencia. Variamos sistemáticamente las condiciones de carga, es decir, el volumen de flujo total, la fracción sólida y la potencia de la corriente, y repetimos cada configuración experimental ocho veces. Se consideraron dos diseños de abanicos aluviales, uno equipado con un canal guía y un puente y otro con el canal guía solamente. En primer lugar, contrastamos la hipótesis de que un régimen de mayor potencia de la corriente del flujo cargado de sedimentos está asociado con una mayor exposición y una menor incertidumbre espacial de la exposición en comparación con flujos generados con una menor potencia de la corriente. En segundo lugar, probamos si un mayor volumen de flujo está asociado con una mayor exposición en el abanico aluvial y con una menor incertidumbre espacial. Ninguna de las hipótesis antes mencionadas se verifica para todo el conjunto de condiciones de flujo. La primera hipótesis se rechaza en la mayoría de las condiciones consideradas. La segunda hipótesis se corrobora predominantemente cuando se consideran las áreas expuestas tanto por sedimentos como por agua. En cambio, cuando se consideran sólo las áreas de depósito de sedimentos, esta hipótesis se corrobora predominantemente en el abanico aluvial que presenta el puente. Proporcionamos mapas de probabilidad de exposición para todas las condiciones experimentales y presentamos la variabilidad de la exposición mediante elipses de desviación estándar. Aunque los resultados cuantitativos de este estudio son concluyentes solamente para los diseños de abanicos aluviales adoptados, ellos, en general, indican que una variación de los parámetros de carga conduce a cambios notables en los patrones de probabilidad de exposición y los parámetros de las elipses de desviación estándar. A la luz de los resultados obtenidos, los tomadores de decisiones deberían tomar en cuenta la variabilidad potencial de las respuestas geomórficas en los abanicos aluviales en sus prácticas de gestión de riesgos para evitar subestimar los impactos en el entorno construido.

Palabras clave: abanico aluvial, peligros fluviales, exposición, modelización.

1. Introduction

Alluvial fans are depositional landforms extending from the locations where the streams leave the mountainous terrain and enter into the receiving waters on the valley floor or debouche into the sea (Bull, 1977). Their dimensions are highly variable both in terms of radial extension and deposition thickness (Bull, 1977; Galloway and Hobday, 1996; Bowman, 2019). Depending on the dominant formation processes, fans can be classified into alluvial and debris flow fans (Blair and McPherson, 1994).

Frequently sediment-laden flows are the main formative processes of alluvial fans (Blair and McPherson, 2009). The variability of these

formative processes is remarkable, either in terms of the composition of the constituting phases (i.e., water, organic and inorganic sediment) or of their magnitude and temporal dynamics (Bowman, 2019). Furthermore, once the flow becomes unconfined on the alluvial fan, a remarkable aleatory uncertainty seems to characterize its distribution and deposition behaviour (Mazzorana *et al.,* 2020; Santibañez *et al.,* 2021; Diaz *et al.,* 2022).

The presence of different geomorphic forms suggests that flow propagation is influenced both by allogenic processes and by interaction with pre-existing morphologies giving rise to autogenic phenomena that may render the geomorphic trajectories even more unpredictable (Clarke, 2015; Diaz *et al.,* 2022). Hence, also the resulting geomorphic patterns will be reminiscent of allogenic (i.e. external forcings on the fan system such as changing climate, glacier lake outburst floods, tectonics, and volcanism) and autogenic controls which Clarke (2015) described as internally derived thresholds within the fan system or process responses (i.e. avulsions and channel migrations) arising from internal feedbacks (Muto *et al.,* 2007).

On alluvial fans, fluvial hazards (i.e. the intensities generated by the ensemble of unfolding flow processes with their associated return periods) may hit in an often rapid and almost unforeseeable manner (National Research Council, 1996) and flood control is a challenging social and engineering endeavor. Nonetheless, the gentle slopes, the open area and the favorable location in terms of sun exposure and water availability make alluvial fans preferred settlement and agricultural areas. Despite ever-increasing investments in structural protection, the flood risk management agencies could not provide a perfectly safe environment for settlement development and the expanding economy (Mazzorana *et al.,* 2014). On the contrary, vicious risk cycles unfolded whenever the additional construction of protective elements induced a perceived sense of safety and prompted further land occupation (Mazzorana *et al.,* 2018). In many regions of the European Alps, significant efforts have been undertaken to provide reliable hazard maps as an essential tool for enhanced spatial planning, aiming at achieving effective risk mitigation (Alexander, 2000; Kienholz *et al.,* 2004; Fuchs, 2009; Bubeck *et al.,* 2016). However, in light of the discussed complexities and interactions of sediment-laden flows on alluvial fans, the following questions arise: (i) How reliable can these assessments be in the context of pronounced process variabilities? (ii) Are there hidden risks (i.e. not considered potential monetary losses) of inhabiting alluvial fan areas declared as safe based on traditional hazard assessments, and in this case, how can these be quantified?

In this context, we contend that the intrinsic variability of distributary processes should be carefully analysed and considered since it could play a crucial role in determining exposure (i.e. the set of assets impacted by the considered hazard processes) on alluvial fans (Whipple *et al.,* 1998; Muto *et al.,* 2007; Van Dijk *et al.,* 2009, 2012). While climate change has been identified as one of the main causes of the ongoing and future increase of exposure to natural hazards (Röthlisberger *et al.,* 2017; De Haas *et al.,* 2018), the aleatory uncertainty associated with distributary processes on alluvial fans has not yet been sufficiently accounted for by flood risk managers (Santibañez *et al.,* 2021; Diaz *et al.,* 2022). If distributary processes on alluvial fans exhibited, at least partially, a random behaviour, the implications for risk assessment would be far-reaching. On the one hand, it would be necessary to find suitable ways to incorporate this variability into deterministic simulations and, on the other hand, additional experimental studies would be deemed as necessary to point out the process pattern diversity to be expected.

Recently, Mazzorana *et al.* (2020) provided experimental evidence that the loading conditions of alluvial fans in terms of supplied flow and sediment volumes have a remarkable influence on exposure. The obtained results indicated that autogenic distributary processes

play a crucial role in determining the exposure of alluvial fans corroborating previous findings of Whipple *et al.* (1998), Muto *et al.* (2007), and Van Dijk *et al.* (2009). They conceded, however, that the experimental program foresaw only one experiment for each parameter set of the considered loading variables and that this limitation could have overshadowed the potential variability of hazard process patterns associated with repeated experiments under experimentally indiscernible loading conditions (Church *et al.,* 2020). To address this issue Santibañez *et al.* (2021) adopted the same experimental setup and alluvial fan layout and repeated each experimental configuration eight times considering also large wood (LW) as part of the flow mixture. In that study, however, the effects of a guiding channel on exposure were not analysed. Santibañez *et al.* (2021) could provide experimental evidence that the variability of hazard processes associated with repeated experiments under experimentally indiscernible loading conditions is, indeed, remarkable and that the water release mode and the fixed proportion of LW exert a decisive effect on these patterns. No specific geostatistical analyses were performed to study the hazard process variability discerning spatial patterns and associating them with the applied loading conditions.

The first step in this direction was attempted by Diaz *et al.* (2022). The performed experimental program was analogous to that adopted in Santibañez *et al.* (2021), with the following remarkable differences: i) the experimental alluvial fan was equipped with a curved guiding channel (i.e. establishing a gross analogy with the real setting of the Blanco River in Chaitén located in Chilean Patagonia) and ii) no LW was added to the flow mixture. Diaz *et al.* (2022) generated an exposure probability map for each loading condition, allowing for a visual interpretation of the peculiar spatial differences emerging from repeated experiments under experimentally indiscernible loading conditions.

Our study aims at refining the understanding of how the spatial patterns of exposure, here defined as the alluvial fan area affected by the sediment-laden flow propagation and by sediment deposition only, are associated with the applied loading conditions and how they may be influenced also by the specific topographic characteristics of the alluvial fan (i.e. presence of a guiding channel equipped or not with a crossing superstructure).

For this, we choose an experimental modelling strategy that has been largely adopted also by hydro-geomorphologists to study alluvial fan processes (Hooke, 1968; D'Agostino *et al.,* 2010; Clarke, 2015; Santibañez *et al.,* 2021; Diaz *et al.,* 2022). Following a recent study by Mazzorana *et al.* (2020), we adopt the 'similarity of process concept' originally proposed by Hooke (1968), who stated that natural systems can be reproduced in laboratory settings by treating them "*as small systems in their own right, not as scale models of prototypes*". Thereby, the relation between specific loading conditions and the resulting patterns of exposure is investigated and the complex physics of the process dynamics occurring on a real alluvial fan is not considered using a Froude-scaled experimental setup (see also Mazzorana *et al.,* 2020). On the contrary, important advances could be achieved by applying the aforementioned approach in determining the primary factors influencing alluvial fan dynamics, such as slope (Hooke, 1968; Guerit *et al.,* 2014), avulsion (Bryant *et al.,* 1995; Reitz and Jerolmack, 2012), autogenic processes (Muto *et al.,* 2007; Van Dijk *et al.,* 2012), and risk (Davies *et al.,* 2003).

Our experimental set-up is aimed at studying a general case not related to any particular case-study and, therefore, is tailored at exploring mainly theoretical questions, therefore the specific study aims are: i) detecting exposure on the alluvial fan due to the generated sediment-laden flows, ii) assessing the variability of exposure associated with the specified loading conditions through suitable indices and probability maps, iii) correlating exposure area and probability with the loading conditions (i.e. total flow volume, solid fraction and the water release from the sup-

ply tank), iv) testing specific correlation hypotheses (e.g. a higher exposure is associated with more severe loading conditions), and v) exploring the main spatial characteristics of exposure maps through spatial analysis tools beyond the reach of the studies conducted recently by Santibañez *et al.* (2021) and Diaz *et al*. (2022).

2. Materials and methods

In this section, we describe the experimental model setup and the applied testing program disclosing both the methodological similarities and highlighting the specific differences with previous studies (see Santibañez *et al.,* 2021; Diaz *et al.,* 2022). Further, the analytic steps to quantify the exposure resulting from the propagation of the sediment-laden flows and the delineation of the spatially explicit exposure probabilities are pointed out. Finally, we describe the applied geostatistical methods (i) to establish correlations between loading conditions and exposure variables, (ii) to test the discussed correlation hypotheses and (iii) to analyse how exposure is affected by the distributary patterns of the sediment-laden flows.

2.1. Experimental model setup and testing programme

We adopted a small-scale experimental model setup, which, despite its simplicity, allows the definition and measurement of the system loading and response variables (Mazzorana *et al.,* 2020). The experimental model consists of three movable components: (i) the alluvial fan, (ii) the feeding channel, and (iii) the supply tank. The dimensions of the model are reported in Figure 1. The employed layout features a guiding channel along its symmetry axis. Alluvial areas are laterally plain and the presence or absence of a bridge superstructure crossing the channel situated at 25 cm from the apex is considered. The entire structure of the feeding channel is made of PVC and the channel bed is covered by PEVA, the fan model is made of PVC as well. The fan itself covers an area of 15.3 dm² and the guiding channel consists of three segments. From a water tank with a capacity of 1.5 L, water is manually released to the feeding channel by handling a valve that can take three different positions: (i) closed, (ii) half opened and (iii) fully opened. The released water is conveyed along a feeding channel to the alluvial fan. The longitudinal profile of the feeding channel features halfway a vertical step followed by a horizontal segment, a configuration that provides wedge storage for the supplied sediments and LW which can be mobilized by the water flow. In this way, a flowing mixture consisting of water, sediments and LW is generated. Depending on the proportion of the mixture components, processes ranging from fluvial sediment transport to hyper-concentrated flows are generated. The LW elements are initially positioned transversally on the top of the stored sediment wedge and the fan model presents a non-erodible surface. Two layouts are adopted to conduct the experiments: (i) Layout 0, with the bridge crossing the channel, and (ii) Layout 1, without the bridge.

A camera, model GoPro Hero Session with a photo resolution of 8 megapixels and a video resolution of 1920x1080 pixel at 60 fps, is installed 0.9 m orthogonally above the model base to record the experiments.

The supplied sediment is a mixture of quartz particles (density of 2.58 g/cm³) with a diameter ranging from 1 to 2 mm (μ = 1.53 mm, σ = 0.17 mm). The LW material consists of wooden poles with a length of 4.8 cm (84 % of the channel width), a diameter of 0.3 cm and a density of 0.7 g/cm³. The experiments were conducted with specific combinations of the total flow volume (V) and the sediment fraction (s). Standard total volume (V_S), to which all the results are referred to, was set to 1.0 l, while the volumes 0.7 l and 1.3 l represent the conditions with reduced (V_r) and increased (V_i) total volume. Similarly, the standard solid fraction (S_S) was set to 15 % of V, while the fractions 5 % and 25 % represent the con-

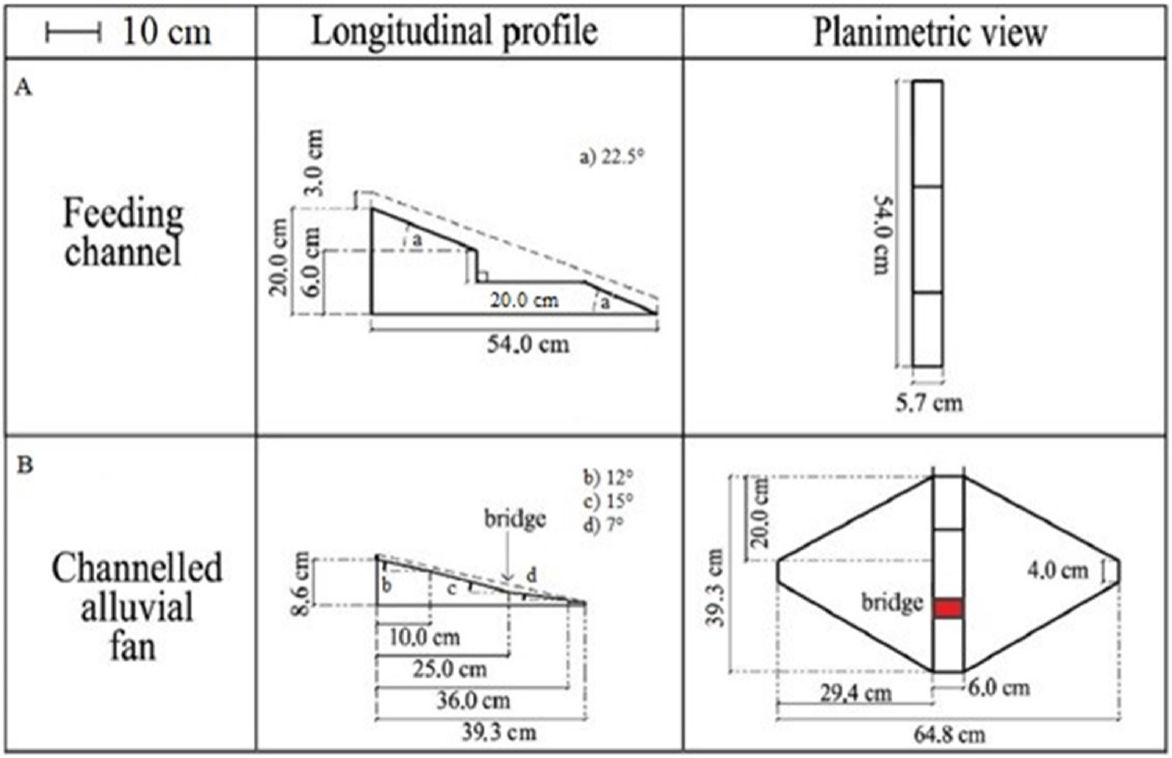

Figure 1. Longitudinal profile (left) and planimetric view (right) of the feeding channel (A) and the artificially channelled alluvial fan model (B) (modified after Mazzorana *et al.,* 2020). Hatched in red: the crossing bridge present in half of the conducted experiments (compare also the experimental programme shown in Figure 2).

Figura 1. *Perfil longitudinal (izquierda) y vista planimétrica (derecha) del canal de alimentación (A) y el modelo de abanico aluvial canalizado artificialmente (B) (modificado según Mazzorana et al., 2020). Sombreado en rojo: el puente cruzante presente en la mitad de los experimentos realizados (compárese también el programa experimental que se muestra en la Figura 2).*

figurations of reduced (S_r) and increased (S_i) solid fraction. The number of supplied LW elements (nlw) was related to the values of VV and s since the LW volume is always 10 % of the total solid volume. Each combination of V and s was repeated with two different water release modes, labelled water release by half-opening the container tap (α_h) and water release by fully opening the container tap (α_f) corresponding to lower and higher average flow rates, respectively. This was accomplished by opening the water container tap at half (45°) or full (90°) rotation, whereby the full rotation approximately led to a halved release time, compared to the half rotation. Each experimental condition was applied to the two fan configurations, Layout 0 with the crossing bridge and Layout 1 without. To assess the variability of the response variables (see Section 2.2) every experimental configuration was repeated eight times (Gschnitzer *et al.,* 2017; Santibañez *et al.,* 2021; Diaz *et al.,* 2022) giving a total number of 288 experimental runs (Figure 2).

Specifically, we employed the same solid fractions as in Santibañez *et al.* (2021), but we adopted an alluvial fan layout that has been previously tested only in Mazzorana *et al.* (2020). In that case, however, only one experimental run was executed for each experimental sediment-laden flow configuration. Hence, the emerging experimental programme is original, although obtained by combining and extending previously adopted designs and experimental configurations.

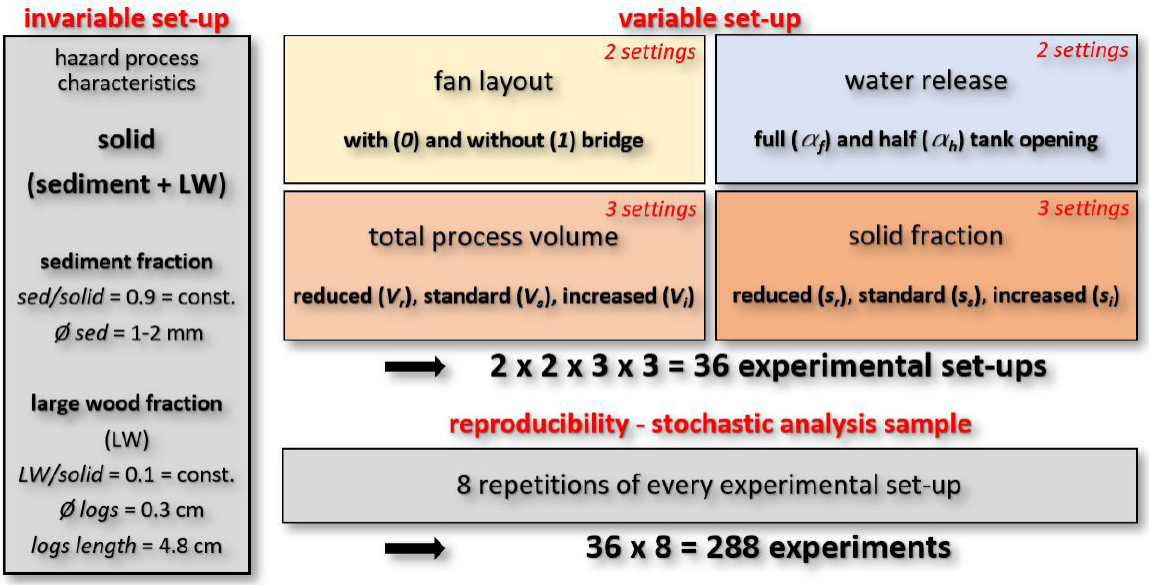

Figure 2. Experimental programme specifying the invariable and variable setup of the conducted experiments. With respect to the latter, we highlight the adopted solid fraction and fan layouts, the water release accomplished by two different tank openings, the total flow volumes, the percentage of the solid fractions within the sediment-laden flow and the number of repetitions (modified after Santibañez *et al.,* 2021 and Diaz *et al.,* 2022).

Figura 2. *Programa experimental que especifica los factores invariables y variables de los experimentos realizados. Con respecto a estos últimos, destacamos la fracción sólida y los diseños de abanico adoptados, la descarga de agua realizada por dos bocas de tanque diferentes, los volúmenes de flujo total, el porcentaje de fracción sólida dentro del flujo cargado de sedimentos y el número de repeticiones (modificado según Santibañez et al., 2021 y Diaz et al., 2022).*

Recently different authors recommended a higher required number of experimental runs for specific fluvial processes and process-structure interactions (Schalko, 2017; Furlan *et al.,* 2019).

An exploratory study on a similar alluvial fan layout by Florin (unpublished) indicates that the number of eight repetitions for each loading condition seems sufficient to reliably capture the variability of the produced process patterns. In the supplementary material (Figure S1) we show the remarkable similarity of the process pattern variability obtained with 8 and 16 repetitions, respectively.

2.1.1. Exposure analysis and probability maps

The detection of exposure on the alluvial fan was accomplished through a series of operations involving the use of two software packages, Anaconda© and ArcGIS© by ESRI. In the first step, the frames from the video recordings of all experimental runs were extracted. Therefore, the videos were processed with a Python script able to obtain a jpg file for every time frame of the analysed video. The jpg file of the last time frame was selected for further analysis since we are particularly interested in detecting the maximum total exposure due to both, the water and the solid material deposits on the alluvial fan surface. The images were further analysed by using ArcMap to obtain i) the exposure area of the solid material deposits only (E_s), and ii) the exposure area due to the sediment-laden flow as a whole (E_{s+w}), that is the areas wetted by water and covered by solid material deposits.

After delineating a common mask for the fan surface, raster maps were generated for all conducted experiments discerning between pixels covered by the solid fraction (E_s) only

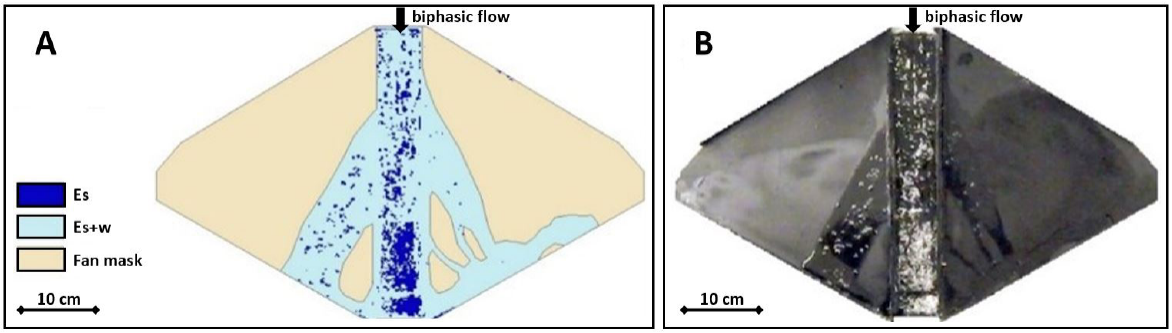

Figure 3. Exposure detection for the experiment with V_i, s_s, α_f, and layout 1. A) Result of the GIS analysis for E_s and E_{s+w}. B) Last time frame.

Figura 3. *Detección de la exposición para V_i, s_s, α_f y el diseño 1. A) Resultados del análisis SIG para E_s and E_{s+w}. B) Captura del último instante.*

and those wetted by the liquid-solid mixture (E_{s+w}) (see Figure 3). Considering the entire set of experiments, a total number of 576 raster maps (288 E_s and 288 E_{s+w}) was obtained. Thus, the exposed areas, E_s and E_{s+w}, are available in form of raster images with two-pixel classes (1 and 0 valued) that identify the exposed (1) and the not-exposed (0) pixels.

Based on the exposure raster maps, the exposure index (i), which is defined as the number of times that a single pixel is exposed throughout the eight repetitions ($0 \leq i \leq 8$), was calculated. The index is expressed in form of percentage assuming the form of the exposure probability EP_i ($EP_i = i/8 \cdot 100$[%]). Subsequently, raster maps showing the exposure probability for every experimental condition in a spatially explicit fashion were generated as in Diaz *et al.* (2022), distinguishing, however, between the exposures E_s and E_{s+w}, respectively (see Figure 4). This analytic step was performed for a total of 72 exposure probability maps in a GIS environment.

While in Diaz *et al.* (2022), spatial analyses focused on obtaining exposure probability maps, further geostatistical investigations are conducted in this study. We subsequently assessed the Exposure Probability Index ($EPI_{v,s}$) for every experimental condition by calculating the sum of the exposure probability of each pixel divided by the total number of pixels. Only alluvial fan areas external to the guiding channel were considered since the exposure to the flow within the channel boundaries is not a harmful condition and thus not relevant in this context. This index is calculated as follows:

$$EPI_{V,s} = \frac{\sum_{i=1}^{8}(px_i \cdot EP_i)}{px_{tot}}\Big|_{V,s} \quad (1)$$

Where: V is the total volume (V_r, V_s, V_i); s is the solid fraction (s_r, s_s, s_i); i is the exposure index; px_i is the number of pixels with exposure index i; EPI_i is the exposure probability at exposure index i; px_{tot} is the total number of pixels of the fan surface minus the pixels belonging to the channel ($px_{tot} = \Sigma px_i - \Sigma px_i|_{channel}$).

We also calculated the Specific Exposure Probability Index ($SEPI$), which accounts only for the pixels that have been exposed at least once during the eight repetitions. This allows referring the randomness of the distributary process to the exposed areas and making the exposure generated under different experimental conditions comparable. By subtracting px_0 (i.e. the number of pixels corresponding to non-exposed conditions in all eight repetitions) from px_{tot} in the denominator, the $SEPI$ can be defined as follows:

$$SEPI_{V,s} = \frac{\sum_{i=1}^{8}(px_i \cdot EP_i)}{px_{tot} - px_0}\Big|_{V,s} \quad (2)$$

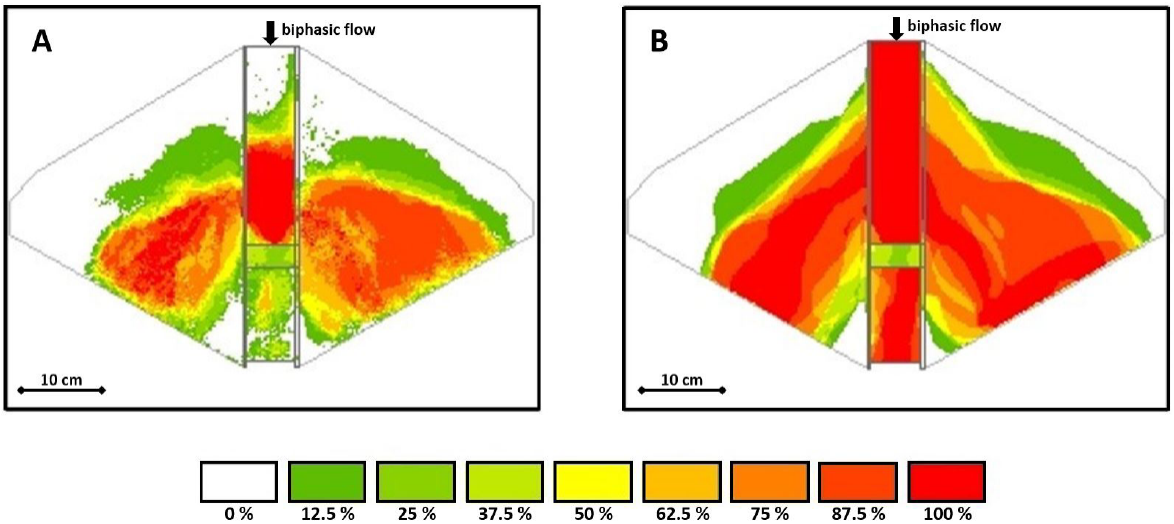

Figure 4. Exposure probability (EP_i) maps associated with the experiment with V_i, s_s, α_h, and layout 0. (A) Exposure index map considering the exposure area of the solid material deposits only (E_s) and (B) exposure area due to the water flow and the solid material deposits (E_{s+w}).

Figura 4. *Mapas de probabilidad de exposición (EP_i) asociados con el experimento con V_i, s_s, α_h, y diseño 0. (A) Mapa del índice de exposición que considera el área de exposición de los depósitos de material sólido únicamente (E_s) y (B) área de exposición debida al flujo de agua y a los depósitos de material sólida (E_{s+w}).*

2.2. Geo-statistical analysis of distributary process patterns

2.2.1. Parameter correlation

To study the statistical relationship between considered input and observed output variables, correlation matrices were determined. These matrices contain the Pearson coefficients r_{xy} defined as follows (Asuero *et al.,* 2006):

$$r_{xy} = \frac{\sigma_{xy}}{\sigma_x \sigma_y} \quad (3)$$

Where: x and y are controlled or measured variables, σ_{xy} is the covariance between x and y, σ_x and σ_y are the respective standard deviations:

$$\sigma_{xy} = \frac{1}{n}\sum_{i=1}^{n}(x_i - x_m)(y_i - y_m) \quad (4)$$

$$\sigma_x = \sqrt{\frac{1}{n}\sum_{i=1}^{n}(x_i - x_m)^2} \quad ; \quad \sigma_y = \sqrt{\frac{1}{n}\sum_{i=1}^{n}(y_i - y_m)^2} \quad (5)$$

The coefficients r_{xy} were calculated to quantify the linear relationship between every controlled input parameter (V, s, nlw) and the mean value of every output variable (E_s, E_{s+w}, EPI_s, EPI_{s+W}) considering the adopted alluvial fan Layout (0 or 1), the water release mode (α_h, or α_f) and the number of repetitions of every loading condition. The obtained correlations values can be associated with different "correlation strengths" based on the criteria in Table 1 (Hartmann *et al.,* 2018).

Table 1. Correlation strengths between variables depending on the r_{xy} value ranges (modified after Hartmann *et al.,* 2018).

Tabla 1. *Intensidades de correlación entre variables dependiendo de los rangos de valores de* the r_{xy} *(modificado según Hartmann et al., 2018).*

Value range	Linear Relationship	Symbol
0-0.49	Nor/Doubtful Positive	NP
0.5-0.69	Weak Positive	WP
0.7-0.89	Medium Positive	MP
0.9-1.0	Strong Positive	SP

2.2.2. Correlation hypotheses

Generally, traditional knowledge and experience may suggest that exposure is positively related to fluvial hazard magnitude and that, in turn, increased exposure is associated with a lower spatial uncertainty given a more extended coverage of the available alluvial fan area (Wagenaar *et al.,* 2016). We stated two specific hypotheses (H) in this study:

H1: the shorter the water release time generating the flow process (i.e. in other words, the more intense the average flow is), the higher is hazard exposure and the lower its associated uncertainty. In operational terms, this means that for given values of V and s, the exposure area (E) releasing water faster (α_f) is larger than the corresponding value obtained by a slower water release (Φ_h). Further, the $SEPI$ index is comparably higher for a shorter water release time (α_f).

H2: the higher the total flow volume of the fluvial hazard process, the higher is the hazard exposure and the lower its associated uncertainty. In operational terms, this means that for given water release time values (α_h, α_f) and s, the exposure area (E) increases with increasing values of V. Further, the $SEPI$ index associated with a higher total volume is higher than the corresponding $SEPI$ index associated with a lower volume.

The testing of these correlation hypotheses can be traced back, in general, to the comparison of the means of two independent and normally distributed samples and, in particular, to the one-sided test problem. Herein, the Null hypothesis is $\mu_x \geq \mu_y$ and the Alternative hypothesis $\mu_x < \mu_y$. The variances of the samples are both unknown but assumed to be equal ($\sigma_x^2 = \sigma_y^2$). In this specific case, a two-sample t-test is applied, where the variance is estimated quantifying the pooled sample variance S^2. The test statistic $T(X, Y)$ with the standard deviation S follows a t-distribution with $n_1 + n_2 - 1$ degrees of freedom if the Null hypothesis is true.

2.2.3. Standard Deviation Ellipses

The spatial analysis of exposure was conducted by calculating Standard deviation ellipses (SDEs), which represent a measure of the spatial distribution of the studied phenomenon (Lefever, 1926; Yuill, 1971). The reader is referred to the supplementary material for the methodological details (see Section A.1).

3. Results

3.1. Exposure analysis and probability maps

Exposure areas (E_s, E_{s+w}) as a percentage of the total fan area are highlighted in Figures 5 and 6.

Figure 5 shows two boxplot graphs of E_s, one with Layout 0 (upper graph) and one with Layout 1 (lower graph), each one reporting the visual summaries associated with the different experimental conditions. These boxplots visualize the position of the median (i.e. bold horizontal line), the interquartile range (IQR = Q3-Q1, i.e. the height of the box), Q1 – 1.5*IQR and Q3 + 1.5*IQR (i.e. the extremities of the vertical lines attached to the box) and the outliers. The single exposure data points associated with each experimental run belonging to the specific experimental conditions are also shown as small green circles.

As shown in Figure 5 one can see, comparing the medians of exposure associated to each experimental configuration, that their values were always higher when Layout 0 was installed and a fast water release time was imposed by fully opening the container tap. With this experimental configuration also the IQR of exposure was larger in almost all cases. The sole exception is IIF0. Releasing water more slowly, no clear absolute dominance is attributable to a specific alluvial fan layout, although with Layout 0 the exposure values are higher in 6 out of 9 experimental configurations and in 4 of them also the IQR is larger.

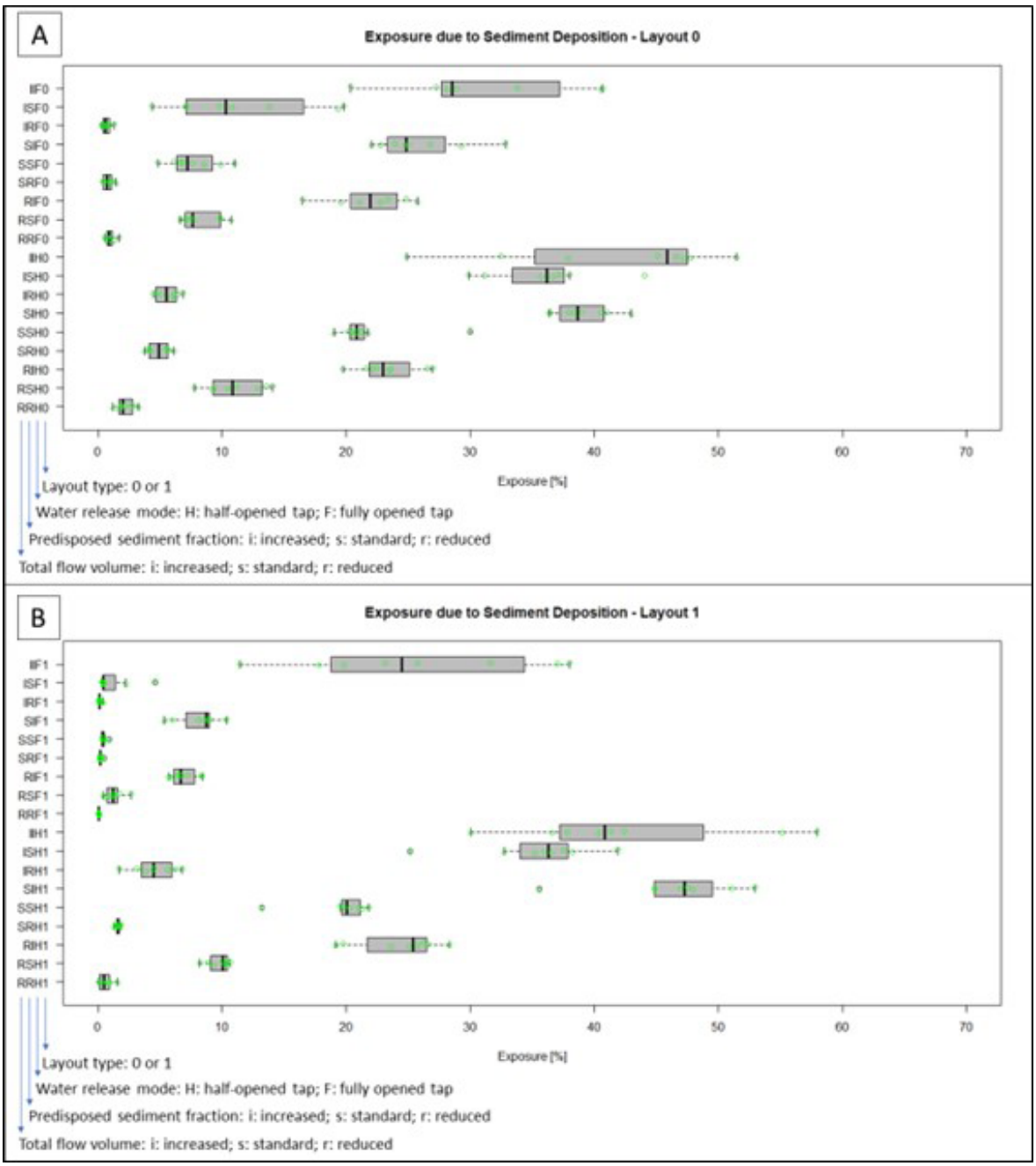

Figure 5. Boxplots for the Layouts 0 (Panel A) and 1 (Panel B), reporting the degree of dispersion and skewness of E_s (i.e. minimum, lower quartile, median, upper quartile and maximum) associated with the different experimental conditions, that is discerning between different levels of released total volume (i.e. V_r, V_s, and V_i), predisposed solid fractions (i.e. s_r, s_s, and s_i) and the imposed water release mode (α_f, α_h).

Figura 5. *Diagramas de caja para los Diseños 0 (Panel A) y 1 (Panel B), que proporcionan el grado de dispersión y sesgo de E_s (es decir, mínimo, cuartil inferior, mediana, cuartil superior y máximo) para las diferentes condiciones experimentales, distinguiendo entre diferentes niveles de volumen total liberado (es decir, V_r, V_s, and V_i), fracciones sólidas predispuestas (es decir, s_r, s_s, and s_i) y el modo de descarga de agua impuesto (α_f, α_h).*

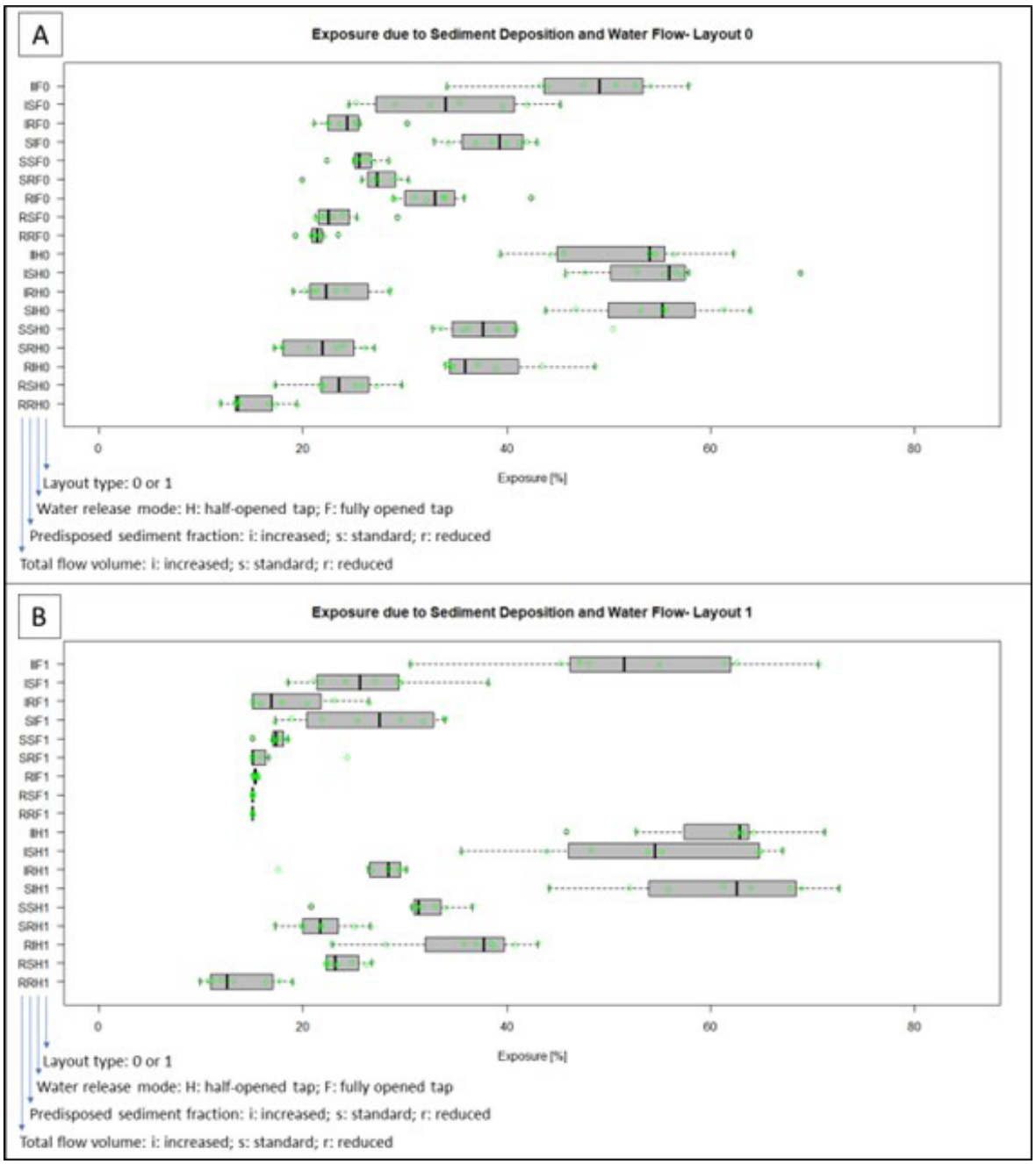

Figure 6. Boxplots for the Layouts 0 (Panel A) and 1 (Panel B), reporting the degree of dispersion and skewness of E_{s+w} (i.e. minimum, lower quartile, median, upper quartile and maximum) associated with the different experimental conditions, that is discerning between different levels of released total volume (i.e. V_r, V_s, and V_i), predisposed solid fractions (i.e. s_r, s_s, and s_i) and the imposed water release mode (α_f, α_h).

Figura 6. *Diagramas de caja para los Diseños 0 (Panel A) y 1 (Panel B), que proporcionan el grado de dispersión y sesgo de E_{s+w} (es decir, mínimo, cuartil inferior, mediana, cuartil superior y máximo) para las diferentes condiciones experimentales, distinguiendo entre diferentes niveles de volumen total liberado (es decir, V_r, V_s, and V_i), fracciones sólidas predispuestas (es decir, s_r, s_s, and s_i) y el modo de descarga de agua impuesto (α_f, α_h).*

On comparing the median values of exposure depending on the water release mode for each alluvial fan layout we observe higher values when the mode of slower water release was set. Keeping the released volume constant and increasing the sediment fraction always resulted in observed increasing exposures (median values). Instead, keeping the sediment fraction constant and increasing the released volume resulted in a more differentiated response. Considering the fully opened (i.e. faster) water release mode on the alluvial fan with Layout 0 only with the increased sediment fraction an increased exposure trend is associated with an increased released total volume. With the same Layout but imposing the half-opened water release mode the increasing exposure trend as a function of the released total volume is observable with the standard and with the increased sediment fraction. Employing Layout 1 with the fully opened water release mode an increase in the released volume increased exposure only when an increased solid fraction was predisposed. Instead, experiments with Layout 1, half-opened water release mode and increasing the released volumes, showed increasing exposure trends when the reduced and standard sediment fractions were apportioned.

As shown in Figure 6 one can appreciate, comparing the medians of exposure associated to each experimental configuration, that the E_{s+w} values were almost always higher when Layout 0 was installed and the fully opened water release mode was imposed. The sole exception is given by releasing an increased total volume and predisposing an increased sediment fraction. Contrarily to the E_s experiments, with this experimental configuration also the interquartile range of exposure is larger only in a subset of cases. In fact, with the release of an increased total volume, two exceptions (i.e. predisposing a reduced and an increased sediment fraction) and with the release on a standard total volume one exception (i.e. with the apportionment of an increased sediment fraction) can be detected.

Setting a half-opened water release mode, no clear absolute dominance is attributable to a specific alluvial fan layout, although with Layout 0 exposure the exposure values are higher in 6 out of 9 experimental configurations. With this experimental setting, the IQR was larger in 5 out of 9 cases. When comparing the exposure (median values) between water release modes for each alluvial fan layout we observe, with alluvial fan Layout 1, higher values when the half-opened water release mode was set. This dominance is less pronounced with alluvial fan Layout 0. Keeping the released volume constant and increasing the sediment fraction almost always resulted in observed increasing exposures (median values). The sole exception can be observed in the conduction of the experiment with the alluvial fan Layout 0 and, specifically, when the half-opened water release mode was imposed and an increased total volume was released. Keeping the sediment fraction constant and increasing the released volume resulted in a more differentiated picture.

Considering shorter water release times (i.e. with the container tap fully opened) on the alluvial fan with Layout 0 only with the standard and with the increased sediment fraction an increased exposure trend is associated with an increased released total volume. With the same Layout but with longer water release times (i.e. half-opened container tap), the increasing exposure trend as a function of the released total volume is observable with the standard and with the reduced sediment fraction. In this experimental configuration, apportioning an increased sediment fraction results in a decreasing exposure when passing from a standard to an increased released volume. Employing Layout 1 an increase in the released volume keeping the predisposed sediment fraction constant resulted almost always in an increase of exposure, irrespective of the employed alluvial fan layout. All only when an increased solid fraction was predisposed. Instead, experiments on the alluvial fan with Layout 1 with a half-opened water release mode and increasing the released volumes, showed increasing exposure

trends when the reduced and standard sediment fractions were apportioned.

In Figure 7 subset of the obtained exposure probability maps is exemplarily shown (i.e. total exposure and sediment exposure respectively) for the standard experimental condition, both alluvial fan Layouts (0 and 1) and both imposed water release modes (α_f, α_h). These maps provide evidence about the inherent experimental variability of the distributary processes on alluvial fans. Clear differences in spatial exposure patterns and probabilities are highlighted due to a change in the water release mode. In both alluvial fan layouts, passing from the half-opened to the fully opened water release mode, is overall associated with less extended exposure areas, both due to water and sediment and solid material deposition areas (see Figure 7), to more extended areas with zero exposure probability and an overall lower mean probability of exposure on both alluvial plains.

In comparison to what is observed with Layout 1, in Layout 0 areas with a high probability of exposure extend further upstream. This pattern appears to be more pronounced when α_h is applied. Figure 7 also evidences that the areas subject to highly variable exposure probability (from 12.5 % to 50 %) constitute mainly "belts" at the borders (but also spots within areas featuring a less variable exposure).

The probability maps corresponding to all experimental conditions (i.e. a total of 72 exposure probability maps) are illustrated in the supplementary material (see Figures S2 to S9).

Figure 8 shows the values of the EPI and the $SEPI$ for all experimental conditions. Firstly, focusing on the EPI values associated with Layout 0, the values obtained by applying the half-opened water release mode α_h are higher than the corresponding values obtained by setting the fully opened water release mode α_f when predisposing the sediment fractions

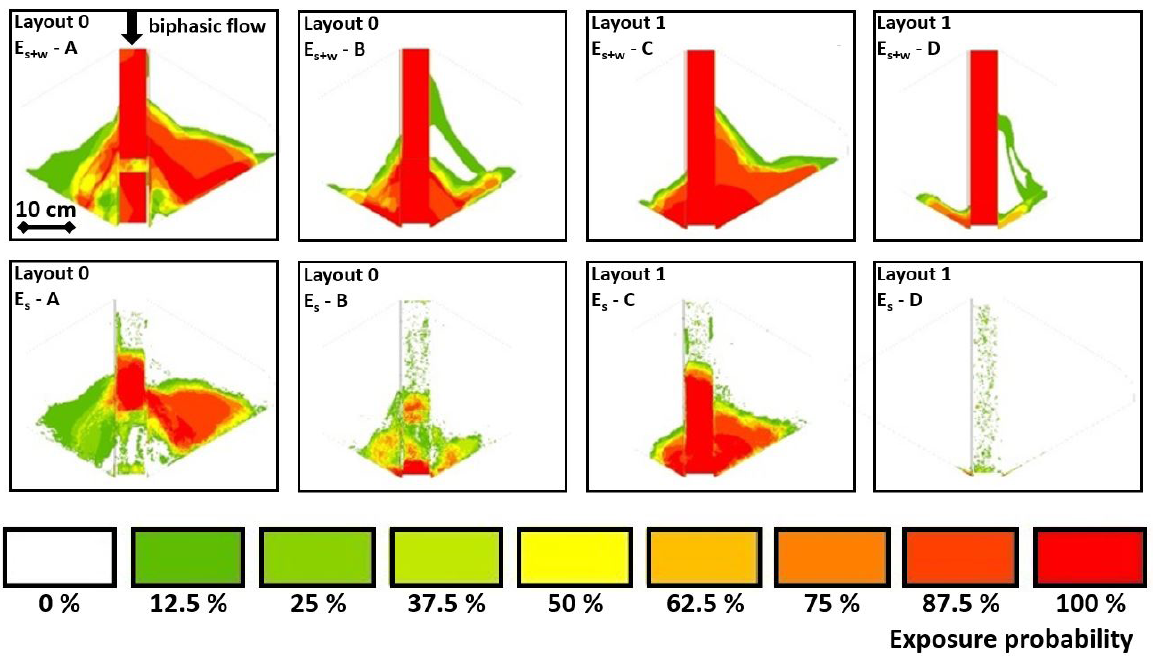

Figure 7. Exposure probability maps relative to the total exposure (E_{s+w}) and sediment exposure (E_s) for the standard experimental condition (V_s, s_s). (A) Layout 0, α_h. (B) Layout 0, α_f. (C) Layout 1, α_h. (D) Layout 1, α_f.

Figura 7. *Mapas de probabilidad de exposición considerando a la exposición total (E_{s+w}) y la exposición debida al depósito de sedimentos (E_s) por la condición experimental estándar (V_s, s_s). (A) Diseño 0, α_h. (B) Diseño 0, α_f. (C) Diseño 1, α_h. (D) Diseño 1, α_f.*

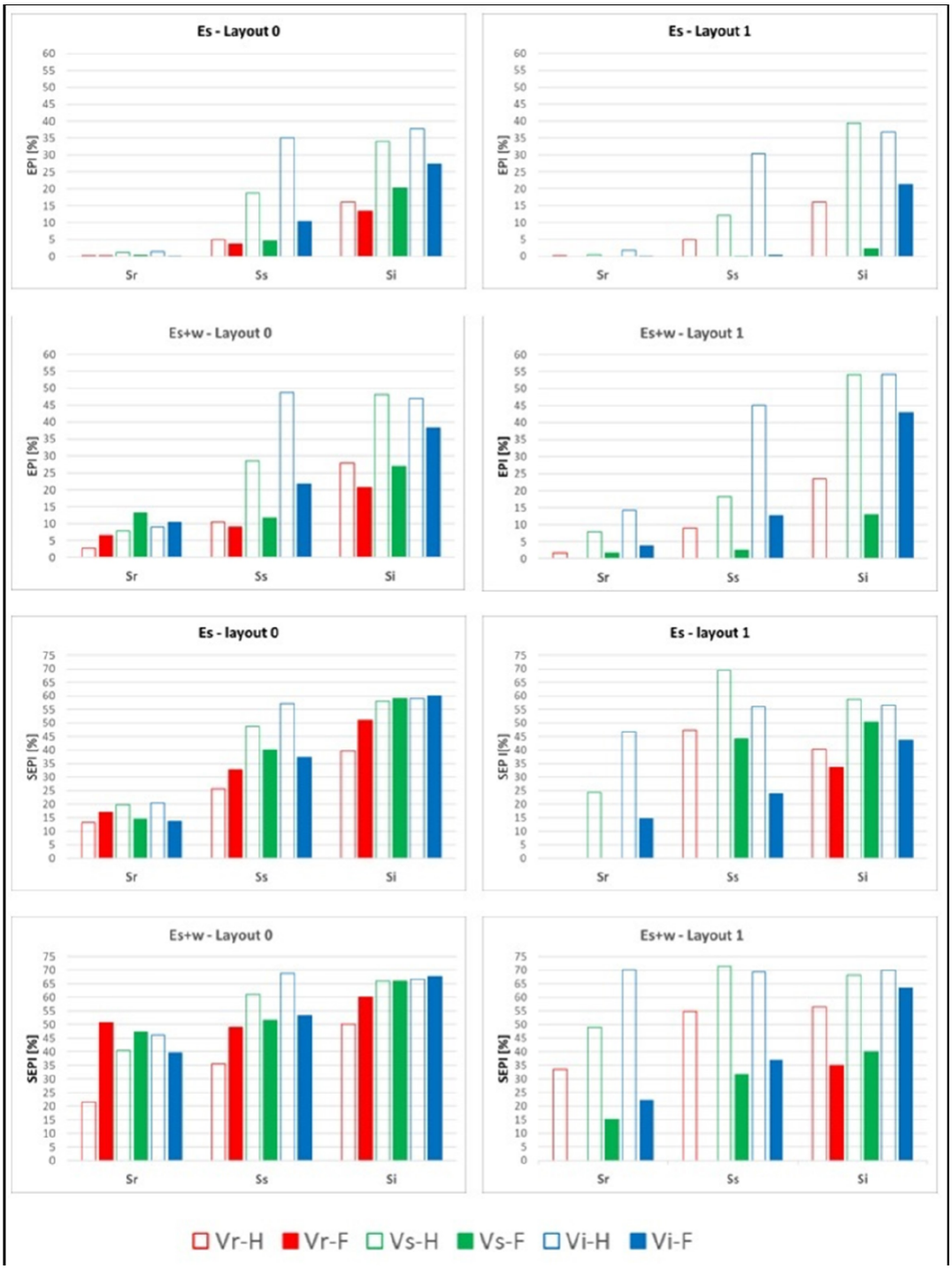

Figure 8. *EPI* and *SEPI* values of the exposure area E_s and the exposure area E_{s+w} relative to the entire set of imposed conditions. Red bars: reduced volume V_r; green bars: standard volume V_s; blue bars: increased volume V_i; empty bars: α_h; full bars: α_f.

Figura 8. *Valores EPI y SEPI del área de exposición E_s y del área de exposición E_{s+w} relativos a todo el conjunto de condiciones impuestas. Barras rojas: volumen reducido V_r; barras verdes: volumen estándar V_s; barras azules: volumen aumentado V_i; barras vacías: α_h; barras plenamente coloradas: α_f.*

s_s and s_i. Instead with s_r, an inverse relationship emerges. Moreover, considering the sediment fractions s_s and s_i, the experiments conducted in the fully opened water release mode α_f exhibit increasing EPI values when releasing increasing total volumes. This is not the case when predisposing s_r. Imposing α_h, EPI values increase strictly with volume with s_r and s_s, but not with s_i since, in this case, the EPI values peak with V_s.

When considering Layout 1, the pattern of the EPI values of the experiments conducted with α_h reflects, with slight magnitude differences, the one from the experiments with Layout 0. Instead in the experiments conducted with the fully opened release mode, EPI values are remarkably lower than the Layout 0 - counterparts, except for the highest total volume (V_l) with the highest sediment fraction (s_l).

The $SEPI$ values obtained for the experiments with Layout 0 show an increasing trend with increasing total volume only when α_h is imposed. Instead, when α_f is set, the $SEPI$ values decrease with increasing total volume if s_r is predisposed, otherwise, the opposite is the case. Overall, when considering Layout 0, neither of the water release modes give rise to remarkably higher $SEPI$ values.

The $SEPI$ bar chart associated with Layout 1 is far less balanced. Generally, the $SEPI$ values obtained by setting the half-opened water release modeα_h are significantly higher compared to those generated by the other release mode. Only with s_i and V_i, the values of this index associated with both water release modes are somewhat close. With α_f, the $SEPI$ values increase augmenting the released total volume within all sediment fraction categories. With α_h, an increasing trend can only be detected in the lowest and highest sediment fraction class.

3.2. Parameter correlation

The Pearson coefficient matrices quantifying the degree of correlation between process loading variables (V, s, nlw) and the mean values of the exposure variables (E_s, E_{s+w}) are reported in the supplementary material (Tables S1 and S2). Here one synthesis table are provided for Layout 0 and one for Layout 1 (see Table 2). There, the intensity of linear

Table 2. Intensity of the linear correlation between hazard and exposure variables for layout 0. NP: no/doubtful positive correlation; WP: weak positive correlation; MP: medium positive correlation; SP: strong positive correlation.

Tabla 2. *Intensidad de correlación lineal entre las variables de carga (peligro hidráulico) y respuesta (exposición) para el diseño 0; WP: correlación positiva débil; MP: correlación positiva de nivel promedio; SP: correlación positiva fuerte.*

Layout 0	**Variables**	E_s	E_{s+w}	EPI_s	EPI_{s+w}
α_h	V	NP	NP	NP	NP
	s	MP	MP	MP	MP
	nlw	SP	SP	SP	SP
α_f	V	NP	NP	NP	NP
	s	SP	MP	MP	MP
	nlw	SP	SP	SP	SP
Layout 1	**Variables**	E_s	E_{s+w}	EPI_s	EPI_{s+w}
α_h	V	NP	WP	NP	WP
	s	MP	MP	MP	MP
	nlw	SP	SP	SP	SP
α_f	V	MP	MP	MP	MP
	s	WP	WP	MP	WP
	nlw	MP	MP	SP	MP

correlation between process loading variables and exposure is determined individually for every applied water release mode (α_f, α_h). The released volume exhibits almost always no or rather a doubtful positive linear correlation with the considered exposure variables except in two cases for Layout 1 with α_h. In these cases, weak correlations with the total flow volume are detected both for the exposure E_{s+w} and the EPI_{s+w}. The sediment fraction exhibits always a moderate positive correlation with the mean values of all exposure variables independently of the Layout and the applied water release mode. When considering Layout 0, the intensity of correlation between the number of wood logs (nlw) and the mean values of all exposure variables is always strong positive. In Layout 1 the strong correlation intensity can be retraced consistently in the experiments with α_h, whereas in the experiments carried out with α_f it is almost medium positive (except between nlw and EPI_s).

Focusing specifically on the effect of the water release mode and calculating the differences of the values of the correlation coefficients between loading variables (V, s, nlw) and the exposure variables (E_s, E_{s+w}), reference is made to the results in Table 3.

Table 3. Differences between correlations at fully opened and half-opened water release modes (α_f, α_h). >: 0.1 – 0.2; >>: larger than 0.2; <: -0.1 – -0.2; <<: less than -0.2; ≈: 0.1 – -0.1.

Tabla 3: *Diferencias entre correlaciones con modo de descarga de agua completamente abierto y semiabierto (α_f, α_h). >: 0.1 – 0.2; >>: mayor que 0.2; <: -0.1 – -0.2; <<: menor que -0.2; ≈: 0.1 – -0.1.*

Layout	Hazard variable	Exposure variable	
		E_s	E_{s+w}
0	V	>>	≈
1		≈	≈
0	s	<	≈
1		>	>>
0	nlw	≈	≈
1		>	>

Applying a half-opened water release mode gives rise to stranger correlations between s and E_s (in Layout 1), nlw and E_s (in Layout 1) and nlw and E_{s+w} (in Layout 1); to bigger differences in the respective values of the correlation coefficients between V and E_s (in Layout 0), s and E_{s+w} (in Layout 1). In the remaining cases, the differences are limited. In Table S3 the effect of the alluvial fan Layout is reported analogously.

3.3. Correlation hypotheses

Recalling the two formulated hypotheses (H1 and H2) and their operationalization in two separated inferences (a and b) to make them testable based on the values of the loading variables and the measured and calculated values of the exposure variables, two statistical inference tables (Tables 4 and 5) are deployed. Herein, first, each operational part of the hypothesis is verified or rejected and the logical AND conjunction of both parts are subsequently evaluated.

From the results of the two separated tests (a and b) associated with H1 and their logical AND conjunction, it emerges (see Table 4) that if E_s is considered as exposure variable the hypothesis that experiments conducted with a fully opened water release mode do not necessarily imply a higher exposure and higher $SEPI$ values. It is statistically corroborated that E_s obtained with α_f is not significantly higher than E_s values associated with α_h. All associated hypotheses are rejected for both alluvial fan Layouts. So, although the operational test b ($SEPI$ value centred hypothesis) is confirmed in a subset of cases, the overall hypothesis is rejected. When considering E_{s+w} as the exposure variable, H1 is rejected in the majority of the considered experimental configurations. There are, however, some noticeable exceptions (i.e. adopting V_r and s_r in the Layouts 0 and 1 and adopting V_s and s_r in Layout 0).

Table 5 reports the results related to H2. When considering E_s as the exposure variable, keeping the water release mode and the predisposed sediment fraction equal, higher exposure and higher $SEPI_s$ values can be as-

Table 4. Results of testing H1. r: rejected hypothesis; v: a verified hypothesis.

Tabla 4. *Resultados relativos al contraste de H1. r: hipótesis rechazada; v: hipótesis aceptada.*

HYPOTHESIS 1		E_s		E_{s+w}		$SEPI_s$		$SEPI_{s+w}$		$H1_s$		$H1_{s+w}$	
Layout		**0**	**1**	**0**	**1**	**0**	**1**	**0**	**1**	**0**	**1**	**0**	**1**
V_r	s_r	r	r	v	v	v	r	v	r	r	r	v	v
	s_s	r	r	r	r	v	r	v	r	r	r	r	r
	s_i	r	r	r	r	v	r	v	r	r	r	r	r
V_s	s_r	r	r	v	r	r	r	v	r	r	r	v	r
	s_s	r	r	r	r	r	r	r	r	r	r	r	r
	s_i	r	r	r	r	v	r	v	r	r	r	r	r
V_i	s_r	r	r	v	r	r	r	r	r	r	r	r	r
	s_s	r	r	r	r	r	r	r	r	r	r	r	r
	s_i	r	r	r	r	v	r	v	r	r	r	r	r

Table 5. Results of testing H2. r: rejected hypothesis; v: a verified hypothesis.

Tabla 5. *Resultados relativos al contraste de H2. r: hipótesis rechazada; v: hipótesis aceptada.*

HYPOTHESIS 2		E_s		E_{s+w}		$SEPI_s$		$SEPI_{s+w}$		$H2_s$		$H2_{s+w}$	
Layout		**0**	**1**	**0**	**1**	**0**	**1**	**0**	**1**	**0**	**1**	**0**	**1**
α_h	s_r	v	v	v	v	v	v	v	v	v	v	v	v
	s_s	v	v	v	v	v	r	v	r	v	r	v	r
	s_i	v	r	r	r	v	r	v	v	v	r	r	r
α_f	s_r	r	r	r	v	r	r	r	v	r	r	r	v
	s_s	r	r	v	v	r	r	v	v	r	r	v	v
	s_i	v	v	v	v	v	r	v	v	v	r	v	v

sociated in a statistically underpinned manner to higher released total volumes in the following experimental setups: (i) Layout 0, α_h, all s, and (ii) Layout 0, α_f, s_i. Further, with Layout 0 and α_h, H2 is verified irrespectively of the predisposed s. With Layout 1, H2 is verified only for α_h and s_r.

When focusing on E_{s+w} as the exposure variable, H2 can be rejected only in the following 4 cases: (i) Layout 0, α_h and s_r; (ii) Layout 0, α_f and s_r; (iii) Layout 1, ceteris paribus condition referred to α_h and s_s, and (iv) Layout 1, α_h and s_r. Noticeably with Layout 1, H2 is verified when the fully opened release mode is applied independently of the predisposed s. H2 is verified for both Layouts when the half-opened water release mode is imposed and the lower sediment fraction is predisposed, and for experiments with a fully opened water release mode, when either s_s *or* s_i is predisposed.

3.4. Standard Deviation Ellipses

Figure 9 shows the location of the centers of the SDEs curves. The lower "density" of the centers in the case of Layout 1, at first sight, suggests a higher process variability due to the presence of the bridge. Moreover, some trends can be identified when considering the change of the SDE centers related to the modification of single hazard variables (V and s). Keeping the water release mode unchanged and the total flow volume constant, an increase in s is generally associated with an upstream migration of the centres, except from two configurations: (i) Layout 1, α_f and V_i.

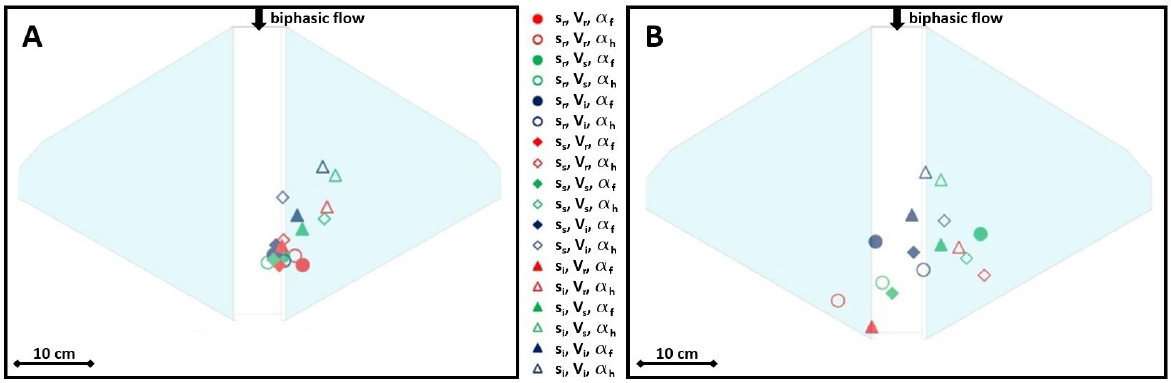

Figure 9. Centres of the SDE curves for the entire set of conditions at layout 0 (A) and 1 (B). Circles, diamonds and triangles represent s_r, s_s, s_i; empty and full symbols represent the α_h and α_f water release mode; red, green and blue represent V_r, V_s, V_i.

Figura 9. *Centros de las EDS (elipses de desviación estándar) para todo el conjunto de condiciones en el diseño 0 (A) y 1 (B). Los círculos, rombos y triángulos representan s_r, s_s, s_i; los símbolos vacíos y llenos representan el modo de descarga de agua α_h y α_f; rojo, verde y azul representan V_r, V_s, V_i.*

where the center of the distribution obtained by setting s_r is located further upstream than the center of the distribution obtained predisposing s_s, and (ii) Layout 1, α_f and V_s, where the center of the distribution obtained by setting s_r is located further upstream than the centres resulting from experiments conducted by predisposing s_s and s_i. The same effect is given by an increase of V while keeping the water release mode unchanged and the solid fraction constant. Also, in this case, two exceptions can be noticed: (i) Layout 1, α_f and s_r, where the V_s centre is slightly upper than the V_r centre, and (ii) Layout 0, α_h and s_r, where the V_d centre is slightly upper than then V_i centre.

In Figure 10 the higher variability in shape and direction of the SDEs associated with Layout 1 compared to the ones associated with Layout 0 is visualized. Moreover, the trend by which SDEs migrate upstream and closer to the apex when increasing either V or s is confirmed. An important parameter to analyse the spatial distribution of the SDEs is eccentricity. Generally, eccentricity decreases with increasing s but not all the cases confirm this trend. In both Layouts 0 and 1, this behaviour is confirmed for conditions generated by setting the half-opened water release mode that also feature a stronger upstream migration of the SDE centers.

4. Discussion and Conclusions

4.1. General statements: compelling evidence for process randomness

Regarding the adopted experimental approach, we reiterate that the setup of the accomplished experiments is based on the similarity of process-concept and a small model extent, which has been used in modified fashions in previous studies (compare Hooke, 1968; D'Agostino *et al.,* 2010; Clarke, 2015; Mazzorana *et al.,* 2020; Santibañez *et al.,* 2021; Diaz *et al.,* 2022). As extensively discussed in these studies, a quantitative representation of sediment transport processes in unconfined natural conditions is necessarily limited. When referring to Froude similarity the applied scale of the model would indeed lead to noticeable scale effects, both concerning the flow and sediment transport behaviour. Geometrical conditions as typical for natural conditions, e.g. surface roughness and detailed bridge structures, or as well grain size of the sediments which are representative for torrential catchments, are not

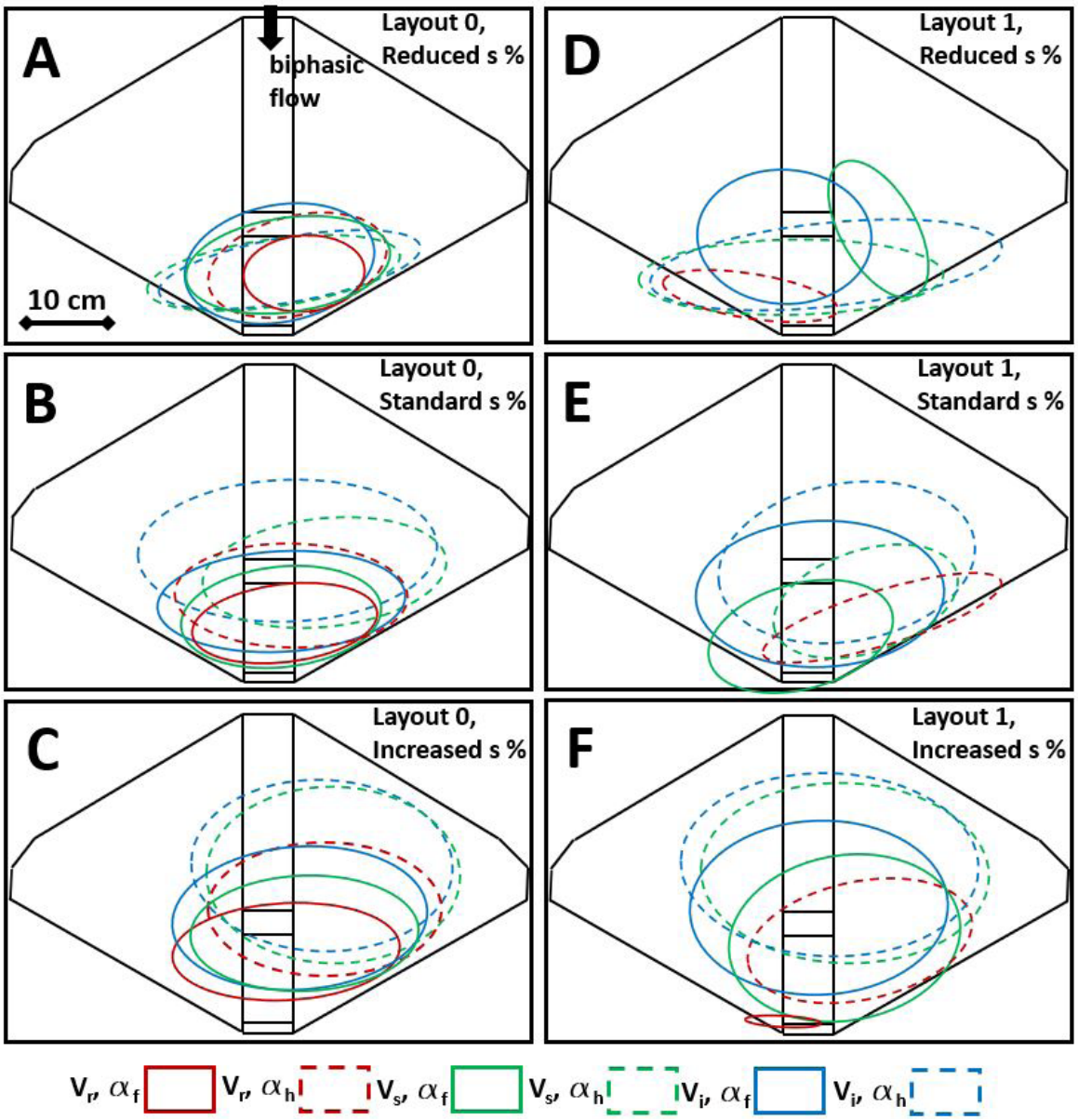

Figure 10. SDEs for all the conditions relative to the total exposure probability (E_{s+w}) of layout 0 (A, B, C) and layout 1 (D, E, F). V_r: reduced flow volume; V_s: standard flow volume; V_i: Increased flow volume; F: fully opened water release mode; H: half-opened water release mode.

Figura 10. *EDS (elipses de desviación estándar) para todas las condiciones relativas a la probabilidad de exposición total (E_{s+w}) del diseño 0 (A, B, C) y diseño 1 (D, E, F). V_r: volumen de flujo reducido; V_s: volumen de flujo estándar; V_i: Volumen de flujo aumentado; F: modo de descarga de agua completamente abierto; H: modo de descarga de agua semiabierto.*

even replicable (Church *et al.,* 2020). However, also with this very simplified experimental set-up and based on the obtained results, we conclude that a kind of randomness of exposure generated by sediment-laden processes at unconfined conditions has to be expected also in large-scale physical models or natural conditions (Paola *et al.,* 2009). Randomness can for instance be caused by marginal changes of grain size during the hazard event, by

a single boulder being mobilized, or by any other minor fluctuations of model boundary conditions, which could influence the system in a way of a tipping point, so that deposition patterns and exposure change. Even though it is not possible to comprehensively analyse the dimension of randomness with this small-scaled model, the results indicate that this randomness generally exists, thereby further corroborating the general findings of Santibañez *et al.* (2021) and Diaz *et al.* (2022).

Another study on fluviatile hazard processes on a torrential fan (Moser, 2018), which comprised several complex experiments on a large Froude-scaled (1:30) model, confirms this hypothesis: Figure 11 illustrates results of experiments for the fan of the Schnannerbach torrent (Austria). The model accurately reproduced the natural conditions and covered a set of buildings on the torrential fan (Sturm *et al.,* 2018a, 2018b). Sediment deposition patterns of five experiments, each accomplished under experimentally indiscernible initial and boundary conditions, are presented. By referring to one experiment as a reference case, the differences in sediment deposition at the end of the experiments are indicated by spatial patterns of differences. In this regard, we argue that establishing experimentally indiscernible boundary conditions, being only almost identical, inevitably introduces a root cause of apparent randomness, whose influence can be limited but not eliminated, by improving both the accuracy and precision of the experiments.

While the small and simplified model in the present study allows a large number of experiments with limited effort and thereby gives a qualitative insight into the stochastics of sediment and LW transport and exposure only on a specific alluvial fan like topography featuring a longitudinal channel with and without

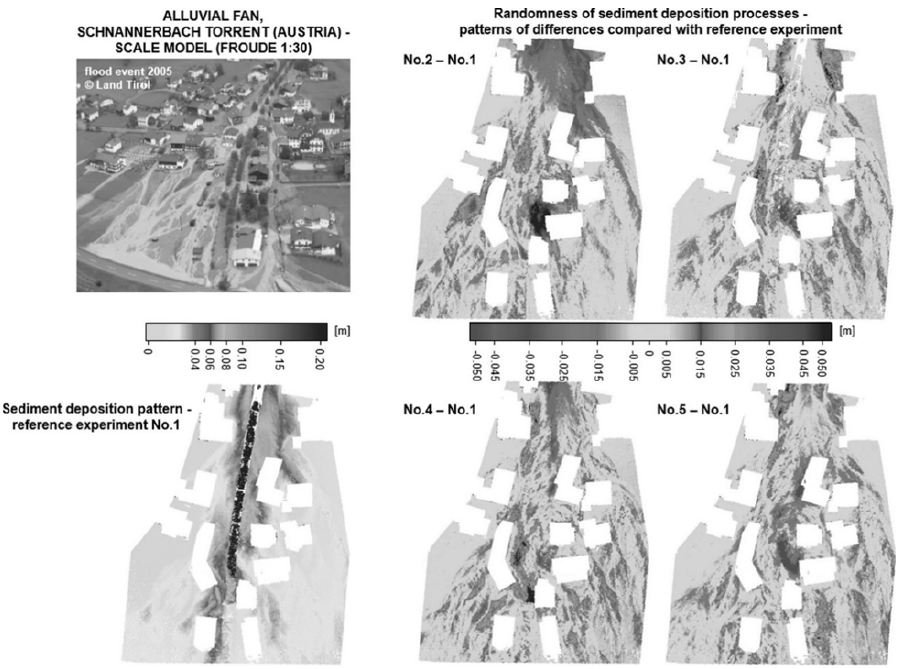

Figure 11. Patterns and spatially distributed differences of sediment depositions at the fan of Schnannerbach torrent (Austria) – results from experiments with a large Froude-scale physical model (1:30) (Sturm *et al.,* 2018a, 2018b; modified after Moser, 2018).

Figura 11. *Patrones y diferencias espacialmente distribuidas de las deposiciones de sedimentos en el abanico del Río Schnannerbach (Austria): resultados de experimentos con un modelo físico de gran tamaño a escala de Froude (1:30) (Sturm et al., 2018a, 2018b; modificado según Moser, 2018).*

a crossing superstructure, larger and more complex models represent the natural conditions more accurately and thus deliver also more robust results. However, only a small number of tests can be managed with reasonable efforts. With this, any statistical analyses could have a limited validity as Schalko (2017) and Furlan *et al.* (2019) pointed out in their studies. So, both types of experiments, either based on the similarity of process-concept or Froude-similarity, despite their specific limitations, can conjointly contribute to a better understanding of the stochastic behaviour of sediment-laden processes in unconfined conditions on alluvial fans (Sturm *et al.,* 2018a, 2018b; Diaz *et al.,* 2022). In light of the foregoing, it seems reasonable to employ the similitude by process approach to detect which experimental settings (i.e. flow conditions and specific unconfined topographies) have the potential to generate markedly stochastic distributary dynamics. In such cases, it may be advisable to foresee a sufficient number of experimental repetitions for the same conditions also on large Froude-scaled models, thereby capturing the emerging process randomness accordingly (compare Schalko, 2017; Furlan *et al.,* 2019).

It is often asserted that only calibrated computational flow models guarantee a high degree of accuracy of the performed simulations as a requisite for reliable hazard and risk assessments (Nguyen *et al.,* 2020). In light of the potential randomness of sediment-laden flows in unconfined flow settings calibration might be extremely challenging. The following argumentations clarify this point.

Let's assume the availability of an extensive set of historical records of extreme events in a thoroughly assessed hydrological context, of carefully documented silent witnesses (watermarks, levees, deposition lobes, grain samples, etc.), of gathered flow data and video-recorded flow patterns (compare also Diaz *et al.,* 2022). Assume furthermore that endowed with these data, the calibration of a validated numerical model (i.e. spatio-temporal match of the propagation patterns of the observed event with the simulated one) is feasible. The calibrated model would then be used with increased confidence in a forward-analysis to deterministically simulate flood hazards with different initial and boundary conditions (i.e. corresponding to prescribed return periods) to provide information for a detailed hazard assessment according to the adopted regional and national standards. But what if rather than being deterministic, process propagation at unconfined landforms such as alluvial fans naturally exhibited an inherently stochastic process behaviour due to the effects of autogenic phenomena? The results from this and other cited studies provide compelling evidence for this. Calibrating, for specified initial and boundary conditions, a computational model to precisely match one particular outcome (i.e. the spatio-temporal process patterns of one specific experimental run) would be misleading in such cases (i.e. remarkable randomness). Any further design endeavour could be affected by significant uncertainties.

4.2. Exposure on alluvial fans: Embracing complexity in light of the compounding effects of imposed experimental conditions and topographic characteristics on process propagation

The peculiarity of descriptive statistical summaries regarding the exposure areas (E_s, E_{s+w}) as a percentage of the total fan area for the imposed boundary conditions and the adopted alluvial fan Layouts as visualized in Figures 5 and 6 urged us to test two specific hypotheses reflecting widespread assumptions in hazard management, namely that: i) a higher average flow rate (i.e. accomplished by the fully opened water release model) of the sediment-laden flow was associated with higher exposure and lower spatial uncertainty of exposure if compared to flows generated by a half-opened water release mode and ii) a higher flow volume was associated with higher exposure on the alluvial fan and with lower spatial uncertainty. In our specific alluvial fan settings, neither of the aforementioned hypotheses could be verified for the whole set

of tested flow conditions. The first hypothesis was rejected in the majority of the considered experimental conditions. The second hypothesis was prevailingly corroborated when the exposed areas due to both sediment and water were considered. Instead, when only the areas of sediment deposition were considered, this hypothesis could be prevailingly corroborated only on the alluvial fan featuring the presence of the bridge.

In synthesis, one cannot expect *a priori* neither that a higher exposure on the alluvial fan resulted from imposing more extreme flow conditions nor that the uncertainties within the exposed spots would be less pronounced than the uncertainties associated with flows generated by a half-opened water release mode. Indeed, the topographical characteristics of the alluvial fan definitively play a significant role as also reported by Santibañez *et al.* (2021). This study also corroborates that the presence of a bridge affects the exposure values remarkably. Our hypothesis testing scheme did not consider the role of the number of wood logs (*nlw*). In this respect, the performed correlation analysis highlighted that the interaction of transported LW with the crossing superstructure (i.e. bridge clogging) exacerbated exposure independently of the average flow rate generated the specific water release mode (i.e. strong correlation), whereas in absence of this feature such a decisive effect is retraceable with the half-opened water release mode (i.e. lower average flow rate). When the fully opened water release mode was set, the correlation strength decreased, although remaining medium positive. Regarding the experiments conducted in absence of the bridge, a careful visual inspection of the process dynamics led to the following insights: With the half-opened water release mode, the interaction of LW with the channel boundaries promoted instream sediment deposition throughout the guiding channel, which, in turn, lead to channel outbursts in different locations. On the contrary, during experiments conducted with a fully opened water release mode, LW jammed preferentially in the distal channel reach thereby reducing the channel sector where frequent outbursts could occur.

The sediment fraction always exhibited a moderate positive correlation with the mean values of all exposure variables independently of the Layout and the applied water release mode. This experimental result has to be interpreted carefully.

Given the experimental set-up of the alluvial fan with a rigid floodplain and channel surface, the present analyses of spatial exposure patterns were based on simplified conditions as the focus was on sediment deposition and re-erosion of deposits only (Sturm *et al.,* 2018b). Erosion of the initial, pre-event channel bed and floodplain was disabled mostly for practical reasons, (i) due to constraints in the construction of the model, (ii) the expense in experimentation and (iii) for ensuring perfectly equal starting conditions for all experimental runs. These non-erodible conditions mean a major simplification when comparing to natural alluvial fans, not consisting of any river engineering measures and infrastructure elements such as streets and sealed areas. Even though the focus in the experiments was on events with high sediment concentrations, not causing sediment-limited conditions at any time during the event, channel erosion would be likely to occur at least locally. Regarding the potential effects of channel erosion on the spatial exposure patterns, we expect that increasing erosion would decrease the spatial extent and volume of sediments on the floodplain. Consequently, channel erosion could cause major erosion along the channel confining geomorphic work. Likely, the hypothesis that higher hazard process intensities lead to higher exposure values would not be corroborated in this case. Comparing, however, the experimental set-up to “engineered” conditions at alluvial fans, where channel erosion is often prevented by a rigid channel bed, we assume that the model results are representative. Channel incision was possible only on deposited sediment lobes but not below the fixed alluvial fan surface. Hence, instream channel

deposition entailed a reduction of flow conveyance either partially obstructing the flow section at the bridge or giving rise to aggradation processes in the distal part of the flow channel. Both processes triggered channel outbursts that, at least on a visual judgement, increased exposure. Sturm *et al.* (2018a, 2018b) could observe similar phenomena in their experimental investigations pointing at the importance of detecting channel aggradations accurately to avoid any further increase of the uncertainty of sediment-laden flow hazards on channelized alluvial fans.

In this study, we retraced in detail the patterns of exposure probability and explored the nexus with the experimental conditions and the adopted alluvial fan Layouts through the quantification of specific indices, the visualization of exposure probability maps and geostatistical calculations as, for example, the determination of the parameters of standard deviations ellipses. Although the specific results were indicative only for the adopted alluvial fan Layouts, the patterns of exposure probability and the parameters of the SDEs changed to a significant extent and often in an unexpected way upon altering any of the values of the considered loading parameters.

4.3. Further Implications and conclusions

We contend that fostering tailored research aiming at further unravelling the complexity and hidden variability of sediment-laden flows on unconfined landforms (i.e. alluvial fans) becomes essential for the societies' ability of proactive adaptation (compare Diaz *et al.,* 2022).

A more complete process understanding could arise from an extensive experimental programme aiming at disentangling, on different alluvial fan topographies, the effects of allogenic factors (i.e. boundary conditions) on the occurrence of autogenic phenomena (i.e. avulsion, channel migration etc.) and the distributary behaviour (i.e. emerging alluvial forms), and on how these mutually coevolve (Clarke, 2015). In this context, the contribution of De Haas *et al.* (2018) is foundational for future research efforts to understand the specific role of avulsion phenomena in determining the distributary behaviour.

These considerations have also important implications for hazard mapping and risk assessment and mitigation.

Rather than providing for hazard maps with crisply delimited zone boundaries, it could be advisable to opt for more smoothed representations based on the results of both experimental and computational studies. Based on improved hazard maps, land use planning strategies could appropriately consider the nuances of the variability of process propagation.

In light of the gained insights, risk mitigation design could attempt removing hydraulic bottlenecks which could lead to highly uncertain process patterns. Interventions should increase the buffer capacity for a broader range of process scenarios rather than optimizing the system performance only for a narrowly defined design event (i.e. concerning a specific return period, a defined composition of the flow mixture and a unique, computationally assessed, system response). Hence, exposed systems should be designed to be flexibly adaptable as to maintain a broad range of functionalities also when heavily perturbed by the impacts of sediment-laden flows.

Statements and Declarations

The authors declare that they have NO financial or non-financial interests that are directly or indirectly related to the work submitted for publication. The authors declare that they have NO competing interests.

Acknowledgements

The research was funded by the project ANID/ CONICYT FONDECYT Regular Folio 1200091 "Unravelling the dynamics and impacts of sediment-laden flows in urban areas in south-

ern Chile as a basis for innovative adaptation (SEDIMPACT)" led by Bruno Mazzorana. The results presented in Figure 11 were accomplished in the course of the project "Vulnerability analysis of buildings exposed to torrent hazards – small scale experimental modelling of impacts on buildings and derivation of physics-based vulnerability functions", funded by the Austrian Science Fund (FWF; P27400-NBL). In this context, special thanks also go to Maximilian Moser, who greatly supported these experiments in the hydraulic engineering laboratory at the University of Innsbruck. In addition, we thank Justinne Rybertt for her assistance in editing the manuscript.

References

Alexander, D. (2000). *Confronting Catastrophe*. Dunedin Academic Press Ltd, Edinburgh UK, 288 pp.

Bachi, R. (1963). Standard distance measures and related methods for spatial analysis. *Papers of the Regional Science Association,* 10(1), 83-132. https://doi.org/10.1111/j.1435-5597.1962.tb00872.x

Blair, T.C., McPherson, J.G. (1994). Alluvial Fans and their Natural Distinction from Rivers Based on Morphology, Hydraulic Processes, Sedimentary Processes, and Facies Assemblages. *Journal of Sediment Research,* 64(3a), 450-489. https://doi.org/10.1306/D4267DDE-2B26-11D7-8648000102C1865D

Blair, T.C., McPherson, J.G. (2009). Processes and Forms of Alluvial Fans. In Parsons, A.J., Abrahams, A.D. (editors). *Geomorphology of Desert Environments,* (pp. 413-467). Springer Netherlands. https://doi.org/10.1007/978-1-4020-5719-9_14

Bowman, D. (2019). *Principles of Alluvial Fan Morphology*. Springer, Netherlands, 151 pp. https://doi.org/10.1007/978-94-024-1558-2

Bryant, M., Falk, P., Paola, C. (1995). Experimental study of avulsion frequency and rate of deposition. *Geology,* 23(4), 365-368. https://doi.org/10.1130/0091-7613(1995)023<0365:ESOAFA>2.3.CO;2

Bubeck, P., Aerts, J.C.J.H., De Moel, H., Kreibich, H. (2016). Preface: Flood-risk analysis and integrated management. *Natural Hazards and Earth System Sciences,* 16(4), 1005-1010. https://doi.org/10.5194/nhess-16-1005-2016

Bull, W.B. (1977). The alluvial-fan environment. *Progress in Physical Geography,* 1(2), 222-270. https://doi.org/10.1177/030913337700100202

Clarke, L.E. (2015). Experimental alluvial fans: Advances in understanding of fan dynamics and processes. *Geomorphology,* 244, 135-145. https://doi.org/10.1016/j.geomorph.2015.04.013

Clarke, L.E., Quine, T.A., Nicholas, A. (2010). An experimental investigation of autogenic behaviour during alluvial fan evolution. *Geomorphology,* 115(3-4), 278-285. doi: 10.1016/j.geomorph.2009.06.033

Church, M., Dudill, A., Venditti, J.G., Frey, P. (2020). Are results in geomorphology reproducible? *Journal of Geophysical Research: Earth Surface,* 125(8), e2020JF005553. https://doi.org/10.1029/2020JF005553

D'Agostino, V., Cesca, M., Marchi, L. (2010). Field and laboratory investigations of runout distances of debris flows in the Dolomites (Eastern Italian Alps). *Geomorphology,* 115(3-4), 294-304. https://doi.org/10.1016/j.geomorph.2009.06.032

Davies, T.R.H., McSaveney, M.J., Clarkson, P.J. (2003). Anthropic aggradation of the Waiho River, Westland, New Zealand: microscale modelling. *Earth Surface Processes Landforms,* 28(2), 209-218. https://doi.org/10.1002/esp.449

De Haas, T., Densmore, A.L., Stoffel, M., Suwa, H., Imaizumi, F., Ballesteros-Cánovas, J.A., Wasklewicz, T. (2018). Avulsions and the spatio-temporal evolution of debris-flow fans. *Earth-Science Reviews,* 177, 53-75. https://doi.org/10.1016/j.earscirev.2017.11.007

Diaz, H., Mazzorana, B., Gems, B., Rojas, I., Santibañez, N., Iribarren, P., Pino, M., Iroumé, A. (2022). What do biphasic flow experiments reveal on the variability of exposure on alluvial fans and which implications for risk assessment result from this? *Natural Hazards,* 111, 3099-3120. https://doi.org/10.1007/s11069-021-05169-8

Florin, R. (2022). *Explorando el alcance de la independencia de escala en la modelación física de la dinámica distributiva en un abanico aluvial*. Diploma Thesis, School of Geology, UACh. 92 pp.

Fuchs, S. (2009). Susceptibility versus resilience to mountain hazards in Austria - Paradigms of vulnerability revisited. *Natural Hazards and Earth System Sciences,* 9(2), 337-352. https://doi.org/10.5194/nhess-9-337-2009

Furlan, P., Pfister, M., Matos, J., Amado, C., Schleiss, A.J. (2019). Experimental repetitions and blockage of large stems at ogee crested spillways with piers. *Journal of Hydraulic Research,* 57(2), 250-262. https://doi.org/10.1080/00221686.2018.1478897

Galloway, W.E., Hobday, D.K. (1996). *Terrigenous Clastic Depositional Systems*. Springer, Berlin Heidelberg Germany, 423 pp. https://doi.org/10.1007/978-3-642-61018-9

Gschnitzer, T., Gems, B., Mazzorana, B., Aufleger, M. (2017). Towards a robust assessment of bridge clogging processes in flood risk management. *Geomorphology,* 279, 128–140. https://doi.org/10.1016/j.geomorph.2016.11.002

Guerit, L., Métivier, F., Devauchelle, O., Lajeunesse, E., Barrier, L. (2014). Laboratory alluvial fans in one dimension. *Physical Review E*, 90, 022203. https://doi.org/10.1103/PhysRevE.90.022203

Hartmann, K., Krois, J., Waske, B. (2018). E- Learning Project SOGA: Statistics and Geospatial Data Analysis. Department of Earth Sciences, Freie Universität Berlin. https://www.geo.fu-berlin.de/en/v/soga/index.html

Hooke, R.L. (1968). Model Geology: Prototype and Laboratory Streams: Discussion. *Geological Society of America Bulletin,* 79(3), 391-394. https://doi.org/10.1130/0016-7606(1968)79[391:MGPALS]2.0.CO;2

Kienholz, H., Krummenacher, B., Kipfer, A., Perret, S. (2004). Aspects of integral risk management in practice: Considerations with respect to mountain hazards in Switzerland. *Österreichische Wasser- und Abfallwirtschaft,* 56(3), 43-50.

Lefever, D.W. (1926). Measuring Geographic Concentration by means of the Standard Deviational Ellipse. *American Journal of Sociology,* 32(1), 88-94. https://doi.org/10.1086/214027

Mazzorana, B., Simoni, S., Scherer, C., Gems, B., Fuchs, S., Keiler, M. (2014). A physical approach on flood risk vulnerability of buildings. *Hydrology and Earth System Sciences,* 18(9), 3817-3836. https://doi.org/10.5194/hess-18-3817-2014

Mazzorana, B., Ruiz-Villanueva, V., Marchi, L., Cavalli, M., Gems, B., Gschnitzer, T., Mao, L., Iroumé, A., Valdebenito, G. (2018). Assessing and mitigating large wood-related hazards in mountain streams: recent approaches. *Journal of Flood Risk Management,* 11(2), 207-222. https://doi.org/10.1111/jfr3.12316

Mazzorana, B., Ghiandoni, E., Picco, L. (2020). How do stream processes affect hazard exposure on alluvial fans? Insights from an experimental study. *Journal of Mountain Science,* 17(4), 753-772. https://doi.org/10.1007/s11629-019-5788-x

Moser, M. (2018). *Physikalische Modellversuche zur Frage der Reproduzierbarkeit von Geschiebetransportprozessen am Schwemmkegel eines Wildbaches.* Mater thesis. Unit of Hydraulic Engineering, University of Innsbruck, 185 pp.

Muto, T., Steel, R.J., Swenson, J.B. (2007). Autostratigraphy: A framework norm for genetic stratigraphy. *Journal of Sedimentary Research,* 77(1-2), 2-12. https://doi.org/10.2110/jsr.2007.005

National Research Council (1996). *Alluvial Fan Flooding*. The National Academies Press, Washington, DC United States of America, 1-182. https://doi.org/10.17226/5364.

Nguyen, N.T., He, W., Zhu, Y., Lü, H. (2020). Influence of Calibration Parameter Selection on Flash Flood Simulation for Small to Medium Catchments with MISDc-2L Model. *Water,* 12(11), 3255. https://doi.org/10.3390/w12113255

Paola, C., Straub, K., Mohrig, D., Reinhardt, L. (2009). The "unreasonable effectiveness" of stratigraphic and geomorphic experiments. *Earth-Science Reviews,* 97, 1-43. https://doi.org/10.1016/j.earscirev.2009.05.003

Reitz, M.D., Jerolmack, D.J. (2012). Experimental alluvial fan evolution: Channel dynamics, slope controls, and shoreline growth. *Journal of Geophysical Research - Earth Surface,* 117, F02021, https://doi.org/10.1029/2011JF002261.

Röthlisberger, V., Zischg, A.P., Keiler, M. (2017). Identifying spatial clusters of flood exposure to support decision making in risk management. *Science of the Total Environment,* 598, 593–603. https://doi.org/10.1016/j.scitotenv.2017.03.216

Santibañez, N., Mazzorana, B., Iribarren, P., Rojas, I., Mao, L. (2021). Dinámica distributiva de flujos bifásicos con carga de madera en un abanico aluvial experimental. *Ingenieria del Agua,* 25(2), 145-168. https://doi.org/10.4995/ia.2021.14703

Schalko, I. (2017). Large wood accumulation probability at a single bridge pier. In Ghani (Editor), Proceedings of the 37th IAHR world congress. Kuala Lumpur, Malaysia: IAHR and Usains Holding SDN BHD, 1704-1713.

Sturm, M., Gems, B., Keller, F., Mazzorana, B., Fuchs, S., Papathoma-Köhle, M., Aufleger, M. (2018a). Experimental analyses of impact

forces on buildings exposed to fluvial hazards. *Journal of Hydrology,* 565, 1–13. https://doi.org/10.1016/j.jhydrol.2018.07.070

Sturm, M., Gems, B., Keller, F., Mazzorana, B., Fuchs, S., Papathoma-Köhle, M., Aufleger, M. (2018b). Understanding impact dynamics on buildings caused by fluviatile sediment transport. *Geomorphology,* 321, 45-59. https://doi.org/10.1016/j.geomorph.2018.08.016

Van Dijk, M., Postma, G., Kleinhans, M.G. (2009). Autocyclic behaviour of fan deltas: an analogue experimental study. *Sedimentology,* 56(5), 1569-1589. https://doi.org/10.1111/j.1365-3091.2008.01047.x

Van Dijk, M., Postma, G., Kleinhans, M.G., Kraal, E. (2012). Contrasting morphodynamics in alluvial fans and fan deltas: effect of the downstream boundary. *Sedimentology,* 59(7), 2125–2145. https://doi.org/10.1111/j.1365-3091.2012.01337.x

Wagenaar, D.J., De Bruijn, K.M., Bouwer, L.M., De Moel, H. (2016). Uncertainty in flood damage estimates and its potential effect on investment decisions. *Natural Hazards and Earth System Sciences,* 16(1), 1-14. https://doi.org/10.5194/nhess-16-1-2016

Whipple, K.X., Parker, G., Paola, C., Mohrig, D. (1998). Channel dynamics, sediment transport, and the slope of alluvial fans: Experimental study. *Journal of Geology,* 106(6), 677-693. https://doi.org/10.1086/516053

Yuill, R.S. (1971). The Standard Deviational Ellipse; An Updated Tool for Spatial Description. *Geografiska Annaler: Series B, Human Geography,* 53(1), 28-39. https://doi.org/10.1080/04353684.1971.11879353

Recibido el 31 de julio de 2021
Aceptado el 29 de marzo de 2023

Supplementary material

A1. Calculation of Standard Deviation Ellipses (SDEs)

To calculate an SDE, first, the centre of the exposure index distribution for every experiment was determined. To explain the employed procedure, let us consider a single exposure map and the origin of the Cartesian coordinate system (*x, y*) centred at the fan apex α. The longitudinal fan axis is the x-axis of the Cartesian coordinate system (*x, y*). Then, every pixel k can be considered as a point feature that has three main attributes: the two coordinates of the pixel centre (x_k, y_k) and the assigned value of exposure index (i) ranging from 0 to 8.

Every pixel centre is considered as the statistical unit of a population of n units, where n is the total number of pixels inside the fan area, and outside the channel ($n = px_{tot}$) . The coordinates of the centre of the population, the mean centre, is calculated as the weighted mean of the coordinates of the n points inside the fan:

$$(x_c, y_c) = (\sum_{k=1}^{n} x_k w_k \, , \sum_{k=1}^{n} y_k w_k) \quad (1)$$

Where: n is the total number of pixels, x_k and y_k are the coordinates of the k^{th} pixel's centre and w_k is the weight of the k^{th} pixel, calculated as the ratio between its exposure index and the sum of the exposure indices considering the whole set of pixels:

$$w_k = \frac{i_k}{\sum_{k=1}^{n} i_k} \quad (2)$$

The spatial dispersion of the distribution can be measured by calculating the standard distance (d) (Bachi, 1963) which depends on w_k and the distance of each point from the centre (d_k):

$$d = \sqrt{\sum_{k=1}^{n} w_k d_k^2} \quad (3)$$

$$d_k = \sqrt{(x_k - x_c)^2 + (y_k - y_c)^2} \quad (4)$$

The spatial dispersion of the exposed pixels can also be assessed by d^2, termed the distance-variance, which can be easily decomposed into the two-directional variances σ_x^2 and σ_y^2.

Also, σ_x and σ_y are the quadratic mean errors in the two directions of the spatial distribution. These two parameters depend on the direction of the reference axes used for their calculation, and they change by rotating them. However, since:

$$d^2 = \sigma_x^2 + \sigma_y^2 = \sigma_{x'}^2 + \sigma_{y'}^2 \quad (5)$$

it is possible to find a couple of perpendicular axes (x', y') crossing each other at the mean centre that sets the correlation between the coordinates of the sample units to zero. This coordinate system forms an angle φ with the original coordinate system (*x, y*) that can be calculated as follows:

$$\varphi = \frac{1}{2} \arctan \frac{\sigma_{xy}}{\sigma_x^2 - \sigma_y^2} \quad (6)$$

Where:

$$\sigma_{xy} = cov(x_k, y_k) = \sum_{1}^{n} w_k (x_k - x_c)(y_k - y_c) \quad (7)$$

Thus, the directional variances can be written to the new coordinates system as follows:

$$\sigma^2{}_{x'} = \sigma_x{}^2 cos^2\varphi + \sigma_y{}^2 sin^2\varphi + 2\sigma_{xy} sin\,\varphi \cos\varphi \quad (8)$$

$$\sigma^2{}_{y'} = \sigma_y{}^2 cos^2\varphi + \sigma_x{}^2 sin^2\varphi - 2\sigma_{xy} sin\,\varphi \cos\varphi \quad (9)$$

Finally, from these parameters, the quadratic mean errors ($\sigma_{x'}$, $\sigma_{y'}$) can be obtained in the new coordinate system, which also represents the two axes of the Standard deviation ellipses (SDEs).

Practically, the SDE analysis was conducted using the spatial analysis tool contained in ArcMapTM that extracts SDEs directly from

the EP maps. Once the whole set of EP maps have been processed applying this technique, and the SDEs have been obtained, the geometrical parameters of the SDEs can be used to spatially characterize the exposure probability distribution. Firstly, an analysis of the centres of the SDEs was performed, providing clues concerning the variation of the geographical "gravity centre" of the studied spatial variate (the exposure probability) according to the imposed experimental conditions. The operation consists of transposing the SDEs' centres coordinates (x_c, y_c) onto a Cartesian axis system where the origin is set at the fan apex.

Secondly, the minor and major axes are assessed and, as a function of these geometrical parameters, the eccentricities e of the SDEs are computed. It describes the degree of similarity of the ellipse to a circle, comparing major and minor axes (σ'_x and σ'_y) using the following expression:

$$e = \sqrt{1 - \frac{\sigma'_x{}^2}{\sigma'_y{}^2}}, (\sigma'_x > \sigma'_y) \quad (10)$$

S2. Probability of Exposure Maps in relation to the Number of Repetitions

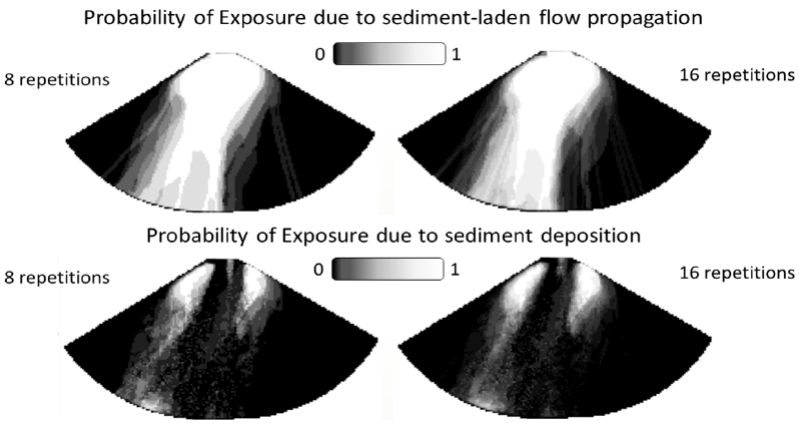

Figure S1. Similarity of the spatial patterns of Probability of Exposure due to sediment-laden flow propagation (see the two upper maps) and due to sediment deposition only (see the two lower maps) obtained on a small-scale alluvial fan with 8 and 16 repetitions, respectively (Florin, unpublished).

Figura S1. *Similitud de los patrones espaciales de la Probabilidad de Exposición debido a la propagación del flujo cargado de sedimentos (ver los dos mapas superiores) y debido a la deposición de sedimentos únicamente (ver los dos mapas inferiores) obtenidos en un abanico aluvial a pequeña escala con 8 y 16 repeticiones, respectivamente (Florin, inédito).*

A3. Spatialized Results

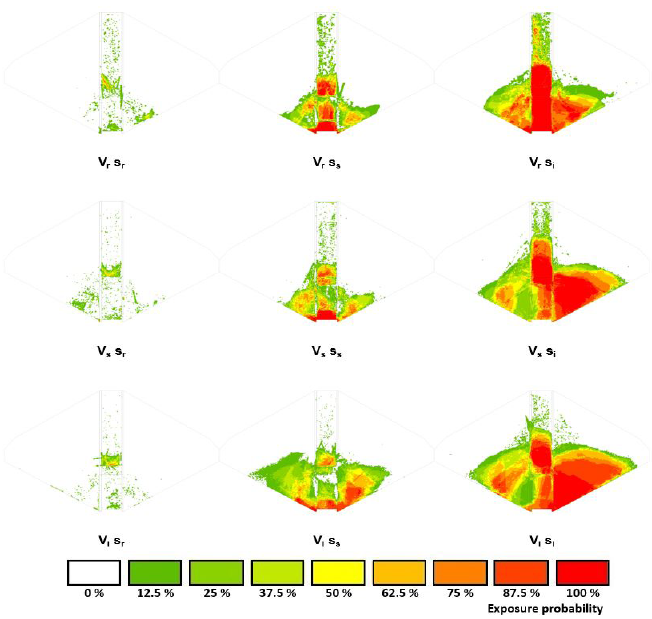

Figure S2. Exposure probability maps relative to the sediment exposure (E_s), Layout 0 and fully opened water release mode for the entire set of imposed loading conditions (i.e. values of the variables V and s).

Figura S2*. Mapas de probabilidad de exposición relativos a la exposición de sedimentos (E_s), diseño 0 y modo de descarga de agua completamente abierto para todo el conjunto de condiciones de carga impuestas (es decir, valores de las variables V y s).*

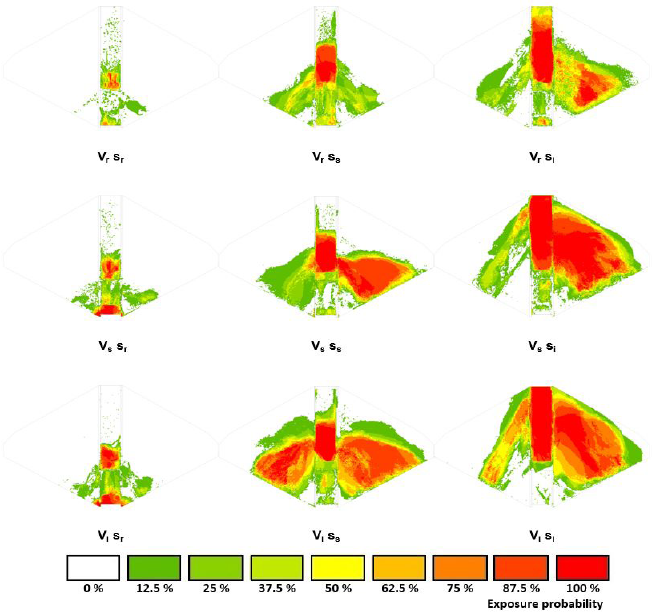

Figure S3. Exposure probability maps relative to the sediment exposure (E_s), Layout 0 and half-opened water release mode for the entire set of imposed loading conditions (i.e. values of the variables V and s).

Figura S3. *Mapas de probabilidad de exposición relativos a la exposición de sedimentos (E_s), diseño 0 y modo de descarga de agua semiabierto para todo el conjunto de condiciones de carga impuestas (es decir, valores de las variables V y s).*

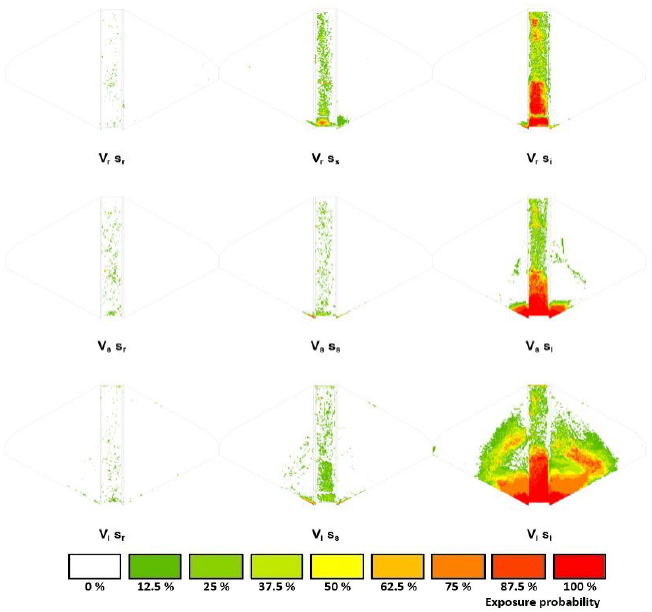

Figure S4. Exposure probability maps relative to the sediment exposure (E_s), Layout 1 and fully opened water release mode for the entire set of imposed loading conditions (i.e. values of the variables V and s).

Figura S4. *Mapas de probabilidad de exposición relativos a la exposición de sedimentos (E_s), diseño 1 y modo de descarga de agua completamente abierto para todo el conjunto de condiciones de carga impuestas (es decir, valores de las variables V y s).*

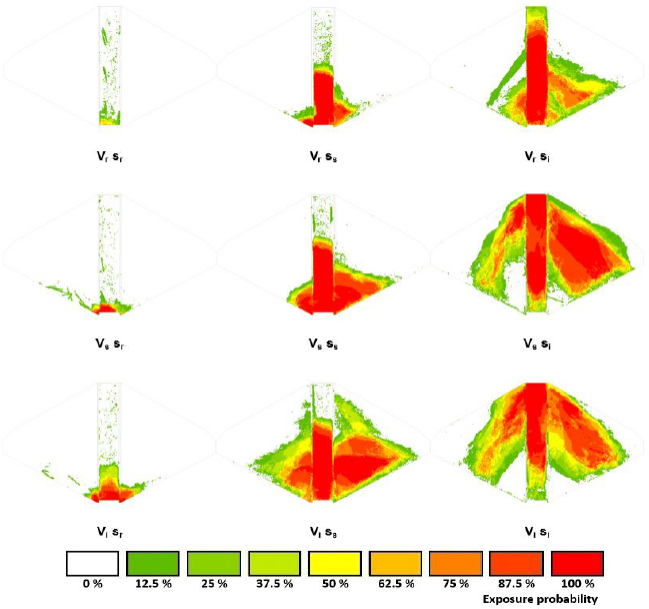

Figure S5. Exposure probability maps relative to the sediment exposure (E_s), Layout 1 and half-opened water release mode for the entire set of imposed loading conditions (i.e. values of the variables V and s).

Figura S5. *Mapas de probabilidad de exposición relativos a la exposición de sedimentos (E_s), diseño 1 y modo de descarga de agua semiabierto para todo el conjunto de condiciones de carga impuestas (es decir, valores de las variables V y s).*

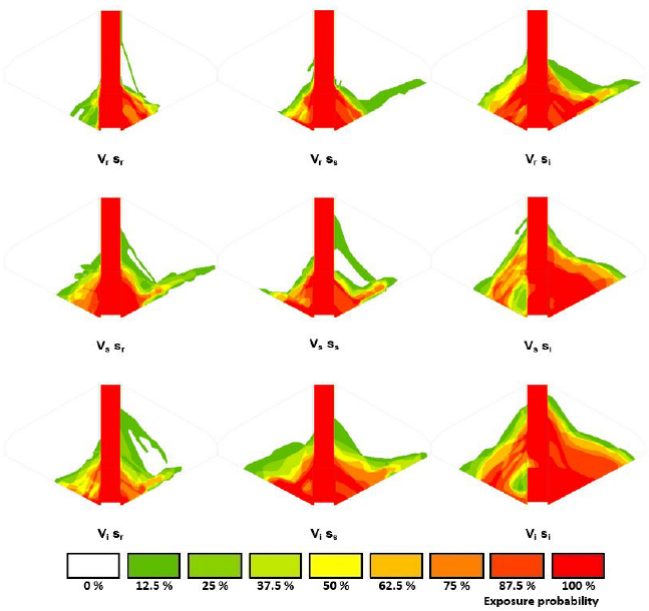

Figure S6. Exposure probability maps relative to the biphasic mixture exposure (E_{s+w}), Layout 0 and fully opened water release mode for the entire set of imposed loading conditions (i.e. values of the variables V and s).

Figura S6. *Mapas de probabilidad de exposición relativos a la exposición generada por la mezcla bifásica (E_{s+w}), diseño 0 y modo de descarga de agua completamente abierto para todo el conjunto de condiciones de carga impuestas (es decir, valores de las variables V y s).*

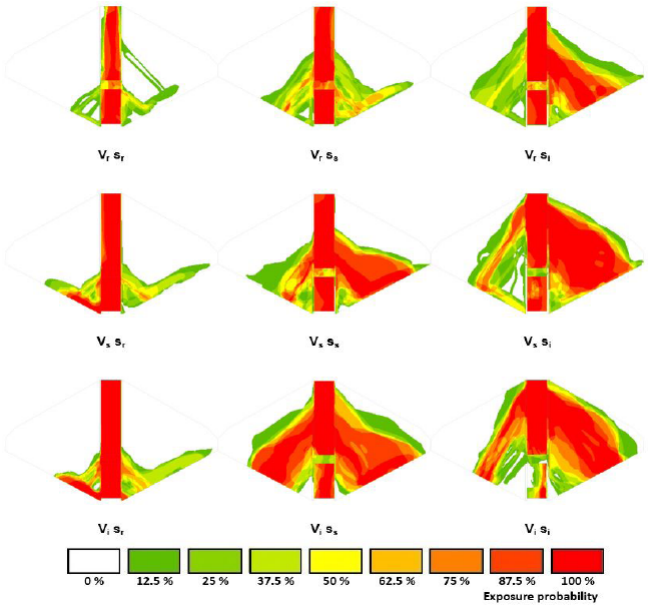

Figure S7. Exposure probability maps relative to the biphasic mixture exposure (E_{s+w}), Layout 0 and half-opened water release mode for the entire set of imposed loading conditions (i.e. values of the variables V and s).

Figure S7. *Mapas de probabilidad de exposición relativos a la exposición generada por la mezcla bifásica (E_{s+w}), diseño 0 y modo de descarga de agua semiabierto para todo el conjunto de condiciones de carga impuestas (es decir, valores de las variables V y s).*

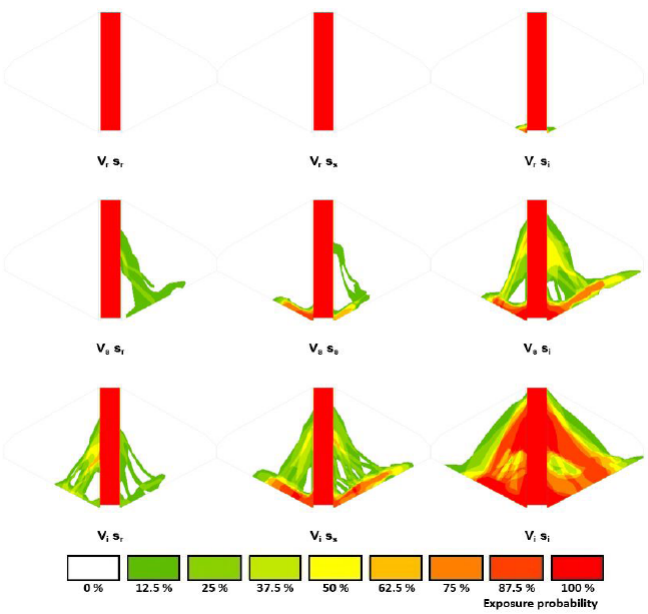

Figure S8. Exposure probability maps relative to the biphasic mixture exposure (E_{s+w}), Layout 1 and fully opened water release mode for the entire set of imposed loading conditions (i.e. values of the variables V and s).

Figura S8. *Mapas de probabilidad de exposición relativos a la exposición generada por la mezcla bifásica (E_{s+w}), diseño 1 y modo de descarga de agua completamente abierto para todo el conjunto de condiciones de carga impuestas (es decir, valores de las variables V y s).*

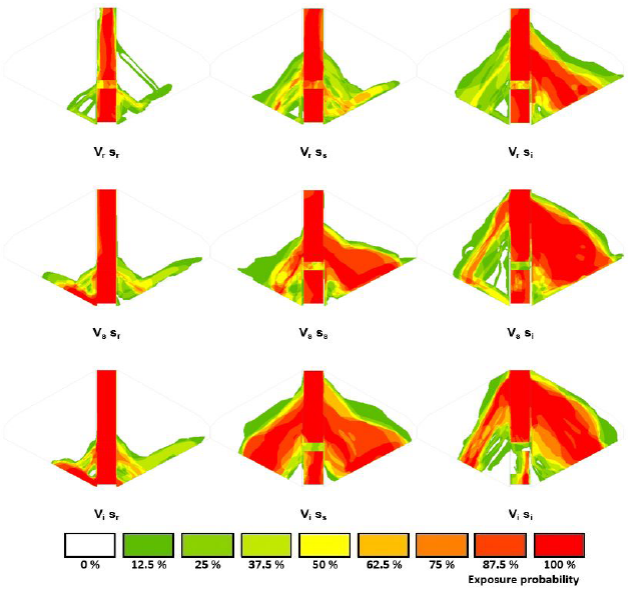

Figure S9. Exposure probability maps relative to the biphasic mixture exposure (E_{s+w}), Layout 1 and half-opened water release mode for the entire set of imposed loading conditions (i.e. values of the variables *V* and *s*).

Figura S9. *Mapas de probabilidad de exposición relativos a la exposición generada por la mezcla bifásica (E_{s+w}), diseño 1 y modo de descarga de agua semiabierto para todo el conjunto de condiciones de carga impuestas (es decir, valores de las variables V y s).*

Table S1. Correlation matrices of the Pearson's coefficient values r_{xy} calculated between hazard (*V, s, nlw*) and exposure (E_s, E_{s+w}) variables for the whole set of considered loading conditions with Layout 0.

Tabla S1. *Matrices de correlación con los valores del coeficiente de correlación de Pearson r_{xy} calculados entre las variables relativas a las condiciones de carga (V, s, nlw) y la exposición (E_s, E_{s+w}) para todo conjunto de condiciones experimentales con el diseño 0.*

Layout 0, α_h	V	s	nlw	E_s	E_{s+w}	EP_E_s	EP_E_{s+w}
V	1	0	0.396	0.433	0.494	0.487	0.486
s	0	1	0.893	0.849	0.784	0.783	0.790
nlw	0.396	0.893	1	0.966	0.907	0.941	0.923
E_s	0.433	0.849	0.966	1	0.982	0.992	0.990
E_{s+w}	0.494	0.784	0.907	0.982	1	0.982	0.997
W	0.466	0.838	0.990	0.983	0.937	0.974	0.954
EP_E_s	0.487	0.783	0.941	0.992	0.982	1	0.992
EP_E_{s+w}	0.486	0.790	0.923	0.990	0.997	0.992	1

Layout 0, α_f	V	s	nlw	E_s	E_{s+w}	EP_E_s	EP_E_{s+w}
V	1	0	0.396	0.151	0.475	0.302	0.479
s	0	1	0.893	0.957	0.787	0.891	0.786
nlw	0.396	0.893	1	0.946	0.941	0.970	0.942
E_s	0.151	0.957	0.946	1	0.913	0.980	0.912
E_{s+w}	0.475	0.787	0.941	0.913	1	0.967	0.99998
W	0.300	0.845	0.935	0.960	0.955	0.988	0.955
EP_E_s	0.302	0.891	0.970	0.980	0.967	1	0.967
EP_E_{s+w}	0.479	0.786	0.942	0.912	0.99998	0.967	1

Table S2. Correlation matrices of the Pearson's coefficient values r_{xy} calculated between hazard (*V, s, nlw*) and exposure (E_s, E_{s+w}) variables for the whole set of considered loading conditions with Layout 1.

Tabla S2. *Matrices de correlación con los valores del coeficiente de correlación de Pearson r_{xy} calculados entre las variables relativas a las condiciones de carga (V, s, nlw) y la exposición (E_s, E_{s+w}) para todo conjunto de condiciones experimentales con el diseño 1.*

Layout 1, α_h	V	s	nlw	E_s	E_{s+w}	EP_E_s	EP_E_{s+w}
V	1	0	0.396	0.390	0.561	0.487	0.560
s	0	1	0.893	0.867	0.771	0.783	0.760
nlw	0.396	0.893	1	0.960	0.937	0.941	0.935
E_s	0.390	0.867	0.960	1	0.974	0.976	0.973
E_{s+w}	0.561	0.771	0.937	0.974	1	0.964	0.998
W	0.437	0.860	0.990	0.982	0.963	0.978	0.963
EP_E_s	0.487	0.783	0.941	0.976	0.964	1	0.963
EP_E_{s+w}	0.560	0.760	0.935	0.973	0.998	0.963	1

Layout 1, α_f	V	S	nlw	E_s	E_{s+w}	EP_E_s	EP_E_{s+w}
V	1	0	0.396	0.323	0.619	0.302	0.616
s	0	1	0.893	0.695	0.527	0.891	0.525
nlw	0.396	0.893	1	0.833	0.821	0.970	0.819
E_s	0.323	0.695	0.833	1	0.914	0.896	0.915
E_{s+w}	0.619	0.527	0.821	0.914	1	0.829	0.99997
W	0.400	0.582	0.784	0.983	0.950	0.836	0.951
EP_E_s	0.302	0.891	0.970	0.896	0.829	1	0.827
EP_E_{s+w}	0.616	0.525	0.819	0.915	0.99997	0.827	1

Table S3. Differences between correlation intensity with Layouts 0 and 1; >: difference between 0.1 and 0.2; >>: difference higher than 0.2; <: difference between -0.1 and -0.2; <<: difference lower than -0.2; ≈: difference between 0.1 and -0.1.

Tabla S3. *Diferencias entre la intensidad de correlación considerando el diseño 0 y 1, respectivamente. >: 0.1 – 0.2; >>: mayor que 0.2; <: -0.1 – -0.2; <<: menor que -0.2; ≈: 0.1 – -0.1.*

Layout 0 vs. 1

Water release mode	Hazard variable	Exposure variable	
		E_s	E_{s+w}
α_f	V	<	<
α_h		≈	≈
α_f	s	>>	>>
α_h		≈	≈
α_f	nlw	>	>
α_h		≈	≈